Title

Metronomic chemotherapy prevents therapy-induced stromal activation and induction of tumor-initiating cells

Journal

Journal of Experimental Medicine, 213(13)

ISSN

0022-1007

Authors

Chan, Tze-Sian
Hsu, Chung-Chi
Pai, Vincent C
et al.

Publication Date

2016-12-12

DOI

10.1084/jem.20151665

Peer reviewed

Metronomic chemotherapy prevents therapy-induced stromal activation and induction of tumor-initiating cells

Tze-Sian Chan,[1,2] Chung-Chi Hsu,[1,4] Vincent C. Pai,[1,4] Wen-Ying Liao,[4] Shenq-Shyang Huang,[6] Kok-Tong Tan,[7] Chia-Jui Yen,[8] Shu-Ching Hsu,[5] Wei-Yu Chen,[3] Yan-Shen Shan,[9] Chi-Rong Li,[1] Michael T. Lee,[10] Kuan-Ying Jiang,[4] Jui-Mei Chu,[4] Gi-Shih Lien,[1,2] Valerie M. Weaver,[11,12,13] and Kelvin K. Tsai[1,4,8]

[1]Graduate Institute of Clinical Medicine, College of Medicine, [2]Laboratory of Advanced Molecular Therapeutics, Division of Gastroenterology, Department of Internal Medicine, Wan Fang Hospital, and [3]Department of Pathology, Wan Fang Hospital, Taipei Medical University, Taipei 11031, Taiwan
[4]Laboratory for Tumor Aggressiveness and Stemness, National Institute of Cancer Research and [5]National Institute of Infectious Diseases and Vaccinology, National Health Research Institutes, Tainan City 70456, Taiwan
[6]Graduate Program of Biotechnology in Medicine, Institute of Molecular and Cellular Biology, National Tsing Hua University, Hsinchu 30013, Taiwan
[7]Department of Surgery, Tung's Metro-harbor Hospital, Taichung 43503, Taiwan
[8]Division of Hematology and Oncology, Department of Internal Medicine and [9]Department of Surgery, National Cheng Kung University Hospital, Tainan 70403, Taiwan
[10]Department of Computer Science, Kun Shan University, Tainan 71003, Taiwan
[11]Department of Surgery, [12]Department of Anatomy, and [13]Department of Bioengineering and Therapeutic Sciences, Center for Bioengineering and Tissue Regeneration, Eli and Edythe Broad Center of Regeneration Medicine and Stem Cell Research, Helen Diller Family Comprehensive Cancer Center, University of California, San Francisco, San Francisco, CA 94143

Although traditional chemotherapy kills a fraction of tumor cells, it also activates the stroma and can promote the growth and survival of residual cancer cells to foster tumor recurrence and metastasis. Accordingly, overcoming the host response induced by chemotherapy could substantially improve therapeutic outcome and patient survival. In this study, resistance to treatment and metastasis has been attributed to expansion of stem-like tumor-initiating cells (TICs). Molecular analysis of the tumor stroma in neoadjuvant chemotherapy–treated human desmoplastic cancers and orthotopic tumor xenografts revealed that traditional maximum-tolerated dose chemotherapy, regardless of the agents used, induces persistent STAT-1 and NF-κB activity in carcinoma-associated fibroblasts. This induction results in the expression and secretion of ELR motif–positive (ELR$^+$) chemokines, which signal through CXCR-2 on carcinoma cells to trigger their phenotypic conversion into TICs and promote their invasive behaviors, leading to paradoxical tumor aggression after therapy. In contrast, the same overall dose administered as a low-dose metronomic chemotherapy regimen largely prevented therapy-induced stromal ELR$^+$ chemokine paracrine signaling, thus enhancing treatment response and extending survival of mice carrying desmoplastic cancers. These experiments illustrate the importance of stroma in cancer therapy and how its impact on treatment resistance could be tempered by altering the dosing schedule of systemic chemotherapy.

The Journal of Experimental Medicine

INTRODUCTION

Solid human tumors such as breast cancer and pancreatic ductal adenocarcinoma (PDAC) are characterized by a pronounced stromal reaction termed the desmoplastic response that can promote tumor progression and aggression (Liotta and Kohn, 2001; Orimo et al., 2005; Karnoub et al., 2007; Shiao and Coussens, 2010). In desmoplastic tumors, carcinoma-associated fibroblasts (CAFs) are a major component of the stroma (Kalluri and Zeisberg, 2006; Erez et al., 2010), and these CAFs are not functionally inert but can foster tumor cell growth, survival, invasion, and even stemness by secreting paracrine factors, such as chemokines (Orimo et al., 2005; Erez et al., 2010), prostaglandins (Rudnick et al., 2011), insulin-like growth factor (Chen et al., 2014), and proteases (Cheng et al., 2002) and by remodeling the extracellular matrix (Serebriiskii et al., 2008; Levental et al., 2009; Goetz et al., 2011). Importantly, both the tumor epithelium and adjacent stroma respond to systemic and local therapies, and a chemotherapy-modified stroma can deleteriously influence

Correspondence to Kelvin K. Tsai: tsaik@tmu.edu.tw or tsaik@nhri.org.tw

Abbreviations used: 3D, three-dimensional; 4H-CPA, 4-hydroxy-cyclophosphamide; ALDH, aldehyde dehydrogenase; α-SMA, α-smooth muscle actin; BLI, bioluminescence imaging; CAF, carcinoma-associated fibroblast; ER, estrogen receptor; FFLuc, firefly luciferase; HSC, hematopoietic stem cell; LCM, laser-capture microdissection; LDM, low-dose metronomic; MDSC, myeloid-derived suppressor cell; MTD, maximum-tolerated dose; PDAC, pancreatic ductal adenocarcinoma; PDX, patient-derived xenografted; PR, progesterone receptor; PSC, pancreatic stellate cells; qRT-PCR, quantitative real-time PCR; SR, super-repressor; TAM, tumor-associated macrophage; TIC, tumor-initiating cell.

The Rockefeller University Press $30.00
J. Exp. Med. 2016 Vol. 213 No. 13 2967–2988
https://doi.org/10.1084/jem.20151665

treatment efficacy (Nakasone et al., 2012; Sun et al., 2012). For instance, chemotherapy can stimulate the infiltration of tumor-associated macrophages (TAMs), myeloid-derived suppressor cells (MDSCs), and endothelial progenitor cells, and these chemo-modified stromal cells secrete inflammatory mediators and proteases, such as IL-1β, CXCR-4, cathepsin B, and matrix metalloproteinase 9, that can compromise therapeutic response (Shaked et al., 2008; Shiao and Coussens, 2010; Gingis-Velitski et al., 2011; Shree et al., 2011; Nakasone et al., 2012; Bruchard et al., 2013; Hughes et al., 2015; Voloshin et al., 2015). Chemotherapy can also enhance the expression of vascular endothelial growth factor on endothelial cells or induce the proliferation and extravasation of intravascular cancer cells and thereby paradoxically promote metastasis (Yamauchi et al., 2008; Daenen et al., 2011). CAFs also respond to chemotherapy, and such antitumor treatments can alter their functionality and endow them with the capacity to promote the malignant behavior of the treated tissue (Sonnenberg et al., 2008). Consistently, CAFs are enriched in chemotherapy-treated human tumor tissues, wherein they promote cancer growth and treatment resistance by secreting paracrine factors such as IL-17A, as was found in colon cancer, and Wnt 16B, as was observed in prostate cancer (Sun et al., 2012; Lotti et al., 2013). Such studies underscore the important role of CAFs in cancer therapy and suggest that targeting this component of the tumor stroma may provide a new avenue to improve the treatment outcome of human malignancies.

Traditional chemotherapy protocols involve the pulsatile administration of drugs to patients at their maximum-tolerated dose (MTD). By comparison, the potential benefit of using comparatively low doses of drug on a more frequent or continuous schedule in chemotherapy, a treatment modality termed low-dose metronomic (LDM) therapy, is slowly becoming appreciated (Kerbel and Kamen, 2004; Pasquier et al., 2010; Loven et al., 2013). Accumulating clinical evidence indicates that LDM chemotherapy offers equal if not better antitumor efficacy than traditional MTD regimens and at a lower accumulative dose of administered drug (Pasquier et al., 2010; Kerbel and Grothey, 2015). Nevertheless, the molecular mechanisms underlying the enhanced treatment response in LDM-treated patients remain poorly understood. In this respect, previous studies that have explored the origins of the enhanced antitumor efficacy of LDM chemotherapy primarily addressed its antiangiogenic effects (Kerbel and Kamen, 2004), such as direct cytotoxicity to endothelial cells (Bocci et al., 2002), reduced recruitment of endothelial progenitor cells and MDSCs into the tumors (Bertolini et al., 2003; Hasnis et al., 2014), and increased expression of the antiangiogenic factor thrombospondin-1 (Bocci et al., 2003). Recent studies suggest that LDM therapy may also mediate its antitumor effect by inhibiting regulatory T cells (Lutsiak et al., 2005; Ghiringhelli et al., 2007) and by triggering the maturation of tumor-infiltrating dendritic cells (Tanaka et al., 2009). Although compelling, these findings were obtained using subcutaneously injected human tumors and consequently were unable to address the impact of CAF–epithelial tumor interactions on the enhanced therapeutic efficacy observed using LDM therapy. Consequently, whether the increased efficacy of LDM treatment could be mediated through an altered CAF response and how remain unclear.

Tumors are highly heterogeneous and likely contain a subset of cancer cells termed tumor-initiating cells (TICs; Visvader and Lindeman, 2008). TICs are intrinsically more resistant to therapy and, consequently, increase disproportionately after systemic chemotherapy and are thought to contribute to tumor relapse and treatment resistance (Li et al., 2008; Visvader and Lindeman, 2008; Creighton et al., 2009). Accordingly, adjuvant strategies that temper the chemotherapy-induced enrichment of TICs could significantly improve the therapeutic outcome of cancer patients. In this regard, TICs exist in a dynamic equilibrium with their microenvironment such that their abundance is tightly regulated by cell–cell interactions and soluble secreted factors such as cytokines (te Poele et al., 2002; Calabrese et al., 2007; Beck et al., 2011; Iliopoulos et al., 2011; Korkaya et al., 2011, 2012). Given that CAFs are an abundant source of cytokines and chemokines and CAFs respond to chemotherapy, we asked whether the treatment-induced enrichment in TICs could be caused by enhanced paracrine signaling induced in CAFs after standard high-dose chemotherapy and whether this phenotype could be tempered by an LDM chemotherapy regimen.

RESULTS

MTD chemotherapy renders CAFs pro-oncogenic

To study the effect of chemotherapy on the interactions between CAFs and their cognate cancer cells in an experimentally controlled manner, we developed a protocol to simultaneously isolate tumor fibroblasts and carcinoma cells from the same freshly excised primary tumors from patients with breast cancer using sequential enzymatic digestion and cell sorting (Fig. 1 A). From a cohort of 15 patients who did not receive preoperative chemotherapy (Table S1), we successfully isolated three pairs of CAFs and carcinoma cells that each could be propagated for at least 15 passages and thereby permitted extensive in vitro and in vivo analysis. After verifying the epithelial origin of the breast carcinoma cells using the marker pan-cytokeratin and the CAFs using the markers CD90 and α–smooth muscle actin (α-SMA; not depicted), we selected two paired cell sets, BCAF-011 (isolated from the tumor of a patient with estrogen receptor [ER]–, progesterone receptor [PR]–, and HER2-negative breast cancer) and BCAF-008 (isolated from a patient with ER-positive, PR-positive, and HER2-negative breast cancer) and their cognate breast epithelial cancer cells BC-011 and BC-008, for further analysis. Both sets of minimally passaged CAFs (less than three passages) were treated with nanomolar concentrations of three standard chemotherapeutic agents, doxorubicin, paclitaxel, or 4-hydroxy-cyclophosphamide (4H-CPA; the

active metabolite of cyclophosphamide), routinely used to treat human breast cancers, and the cells were exposed over time interval and at a dosage that best approximated the mean serum levels achieved in patients, as estimated by pharmacodynamic studies using a standard clinical MTD regimen (50 nM × 96 h, 650 nM × 24 h, and 150 nM × 1 h, respectively; Fig. 1 B; Struck et al., 1987; Twelves et al., 1991; Fogli et al., 2002). Serial monitoring of the treated CAFs revealed early onset (between 3 and 14 d after initiation of the treatments) apoptosis in a population (10–20%) of fibroblasts, whereas the bulk of the treated cells survived that treatment (4 wk) and were found to be growth arrested and express features of senescence and mitotic dysregulations (Fig. 1 C and not depicted).

To explore whether the MTD chemotherapy–treated CAFs (MTD-CAFs) may modulate the behaviors of the neighboring carcinoma cells, we co-cultured the surviving CAFs collected at 2 wk after initiation of the treatments with their cognate carcinoma cells in a three-dimensional (3D) culture assay that recapitulates the tissue-like architecture of breast tumor tissue (Tsai et al., 2005). Notably, when compared with the vehicle-treated CAFs, all pairs of the MTD-doxorubicin–, MTD-paclitaxel–, or MTD–4H-CPA–treated BCAF-011 CAFs substantially enhanced the growth and promoted the invasive behavior of their cognate carcinoma cells (Fig. 1, D–F). The stimulatory effects of MTD-CAFs on cancer cells were consistently observed in other paired BC-008 carcinoma cells and BCAF-008 CAFs and are unlikely to be cancer subtype–specific, as MTD-CAFs also promoted the invasive growth of established breast carcinoma cells, including the basal subtype HCC-1954 cells and the luminal subtype MCF-7 cells (Fig. 1 E).

To examine whether the MTD-treated CAFs could also promote tumor progression and aggression in vivo, we lentivirally transduced the primary BC-011 carcinoma cells with firefly luciferase (FFLuc) and orthotopically inoculated them with vehicle- or MTD-doxorubicin–treated BCAF-011 CAFs at a cancer cell to CAF ratio of 1:2 into the mammary fat pads of immunodeficient NOD/Shi-*scid*/IL2Rγ^{null} (NOG) mice (Fig. 1 G), with the tumors generated by this model recapitulating the histological features, especially the CAF contents (∼40–45%), of the primary human breast cancer they were excised from (Fig. 1 H). In line with the preceding in vitro findings, those tumor cells co-injected with MTD-CAFs grew significantly faster and developed lymph node and pulmonary metastasis at both a higher frequency and with a shorter latency than the tumor cells injected with vehicle-treated CAFs (Fig. 1 I). These findings indicate that MTD chemotherapy endows CAFs with the ability to foster tumor growth and aggression.

MTD-CAFs expand the population of TICs

Our ensuing functional studies revealed that MTD-CAFs not only promoted the invasive growth of the co-cultivated breast carcinoma cells, but also rendered them significantly more refractory to chemotherapy (Fig. 2 A). These observations raised the possibility that the MTD-CAFs may have fostered the expansion of TICs, defined as cells with tumor-initiating and treatment-resistant properties, within the co-injected population of carcinoma cells (Visvader and Lindeman, 2008). To address this possibility, we co-cultivated carcinoma cells with vehicle- or MTD-chemotherapy–treated CAFs within a dual chamber co-culture apparatus. As implied by our in vivo study results, we found that BC-011 carcinoma cells when cultured together with MTD-CAFs, regardless of their inducing agents, contained a higher percentage of $CD44^{+}CD24^{low/-}$ cells, and we determined that this population of cells increased progressively over time (Fig. 2 B and Fig. S1; Al-Hajj et al., 2003; Liu et al., 2014). MTD-CAFs also raised the percentage of $CD44^{+}CD24^{low/-}$ cells in several established breast cancer cell lines (Fig. 2 C). These $CD44^{+}CD24^{low/-}$ carcinoma cells up-regulated mesenchymal cell markers and were highly invasive and had enhanced tumor-initiating potentials both in vitro and in vivo (not depicted). Consistently, breast carcinoma cells co-cultivated with MTD-CAFs exhibited higher tumorsphere-forming abilities in a limiting dilution assay (Fig. 2, E and F). Interestingly, MTD-CAFs also significantly increased the population of cells with high aldehyde dehydrogenase (ALDH) activity ($ALDH^{high}$), which is known to contain another enriched population of TICs (Ginestier et al., 2007), in luminal subtype BT-474 carcinoma cells (Fig. 2 D), albeit to a lesser extent than the increase in the percentage of $CD44^{+}CD24^{low/-}$ cells. Intriguingly, further meticulous cell subpopulation experiments revealed that the $CD44^{+}CD24^{low/-}$ TICs were not derived from the $ALDH^{high}$ cells but were mainly derived from those carcinoma cells that were neither $CD44^{+}CD24^{low/-}$ nor with high ALDH activity (i.e., non-$CD44^{+}CD24^{low/-}$/$ALDH^{low}$ cells, representing more differentiated carcinoma cells) when they were co-cultivated with MTD-CAFs (Fig. 2, G and H). These data suggest that these TICs were likely derived through the dedifferentiation or the reprogramming of differentiated carcinoma cells (Vermeulen et al., 2010; Iliopoulos et al., 2011; Liu et al., 2014; Zhang et al., 2015).

To explore the in vivo significance of the expansion of TICs induced by MTD-CAFs, we lentivirally transduced BC-011 cells with GFP and inoculated them together with vehicle- or MTD-treated CAFs into the mammary fat pads of NOG mice and assessed levels and expansion of TICs within the resultant tumors (Fig. 2 I). Consistent with the notion that MTD-CAFs stimulate the conversion of TICs from within a breast tumor population, we observed that the percentage of $GFP^{+}CD44^{+}CD24^{low/-}$ carcinoma cells substantially increased in those tumors co-injected with MTD- and not vehicle-treated CAFs (Fig. 2 J). These data argue that MTD-CAFs can stimulate the conversion of and support the expansion of TICs within a population of breast carcinoma cells.

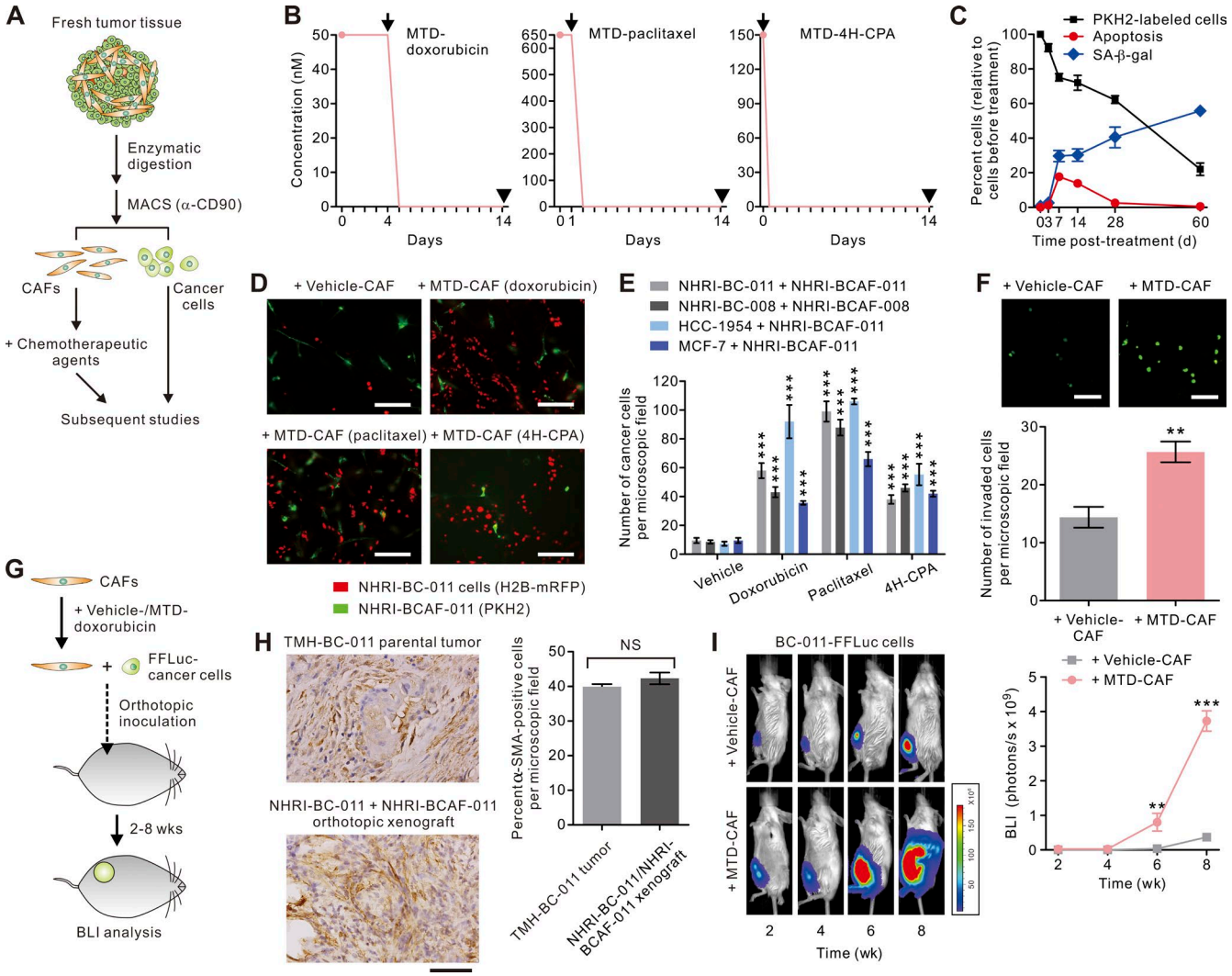

Figure 1. **MTD chemotherapy–treated CAFs are pro-oncogenic.** (A) Schematic illustrating strategy used to prepare primary CAFs or carcinoma cells from fresh human breast cancer for subsequent treatments and analyses. MACS, magnetic-assisted cell sorting. (B) Schematic showing doxorubicin, paclitaxel, or 4H-CPA treatment protocols that mimic MTD chemotherapy regimens in the clinical settings. Arrows indicate time of drug clearance by wash; arrowheads indicate time of analysis (14 d after initiation of the treatments). (C) PKH2-labeled BCAF-011 CAFs were treated with doxorubicin as in B, and the cells were fixed and stained with cleaved caspase-3 (representing apoptotic cells) or senescence-associated β-gal (SA-β-gal; representing senescent cells) at the indicated time after initiation of treatments. Data from two independent experiments ($n = 3$ in each group; mean ± SEM) are shown. (D) Representative immunofluorescence images of BC-011 carcinoma cells lentivirally transduced with monomeric red fluorescence protein (mRFP; red) co-cultivated in 3D multicomponent gels with vehicle-, MTD-doxorubicin–, MTD-paclitaxel– , or MTD–4H-CPA–treated BCAF-011 CAFs (PKH2 labeled; green). Bars, 200 µm. (E) Bar graphs quantifying the number of breast carcinoma cells per image field after 7 d of co-culture with vehicle- or chemo-treated BCAF-011 or BCAF-008 CAFs. Data from three independent experiments ($n = 3$ in each group) are shown. (F) The invasive capacities of BC-011 carcinoma cells in response to vehicle- or MTD-CAFs in a Transwell invasion assay. (Top) Shown are representative immunofluorescence images of the invaded cells, with cell nuclei stained with CYTOX-green dye. Bars, 100 µm. (Bottom) The numbers of invaded cancer cells. Data from three independent experiments ($n = 3$ in each group) are shown. (G) BCAF-011 CAFs were treated with MTD-doxorubicin (MTD-CAF) or vehicle (vehicle-CAF) and then co-injected with FFLuc-transduced BC-011 carcinoma cells into the mammary fat pads of immunodeficient NOG mice. Tumor bulk was monitored using bioluminescence imaging (BLI). (H, left) Representative immunohistochemical images of α-SMA staining in a desmoplastic tumor generated by co-inoculating primary BC-011 breast cancer cells and BCAF-011 CAFs into the mammary fat pads of NOG mice (bottom) and the parental human breast cancer tissue (TMH-BC-011 tumor; top). Bar, 100 µm. (Right) Percent α-SMA–positive cells in the microscopic field. At least 10 different areas were examined in each tissue. Data from three independent experiments are shown. (I, left) Representative BLI of tumors at the indicated time after cell inoculation as described in G. (Right) Tumor bulk quantified as BLI normalized photon counts as a function of time. Data from one experiment ($n = 6$ in each group) are shown. Data are mean ± SEM; Student's t test. **, $P < 0.01$; ***, $P < 0.001$.

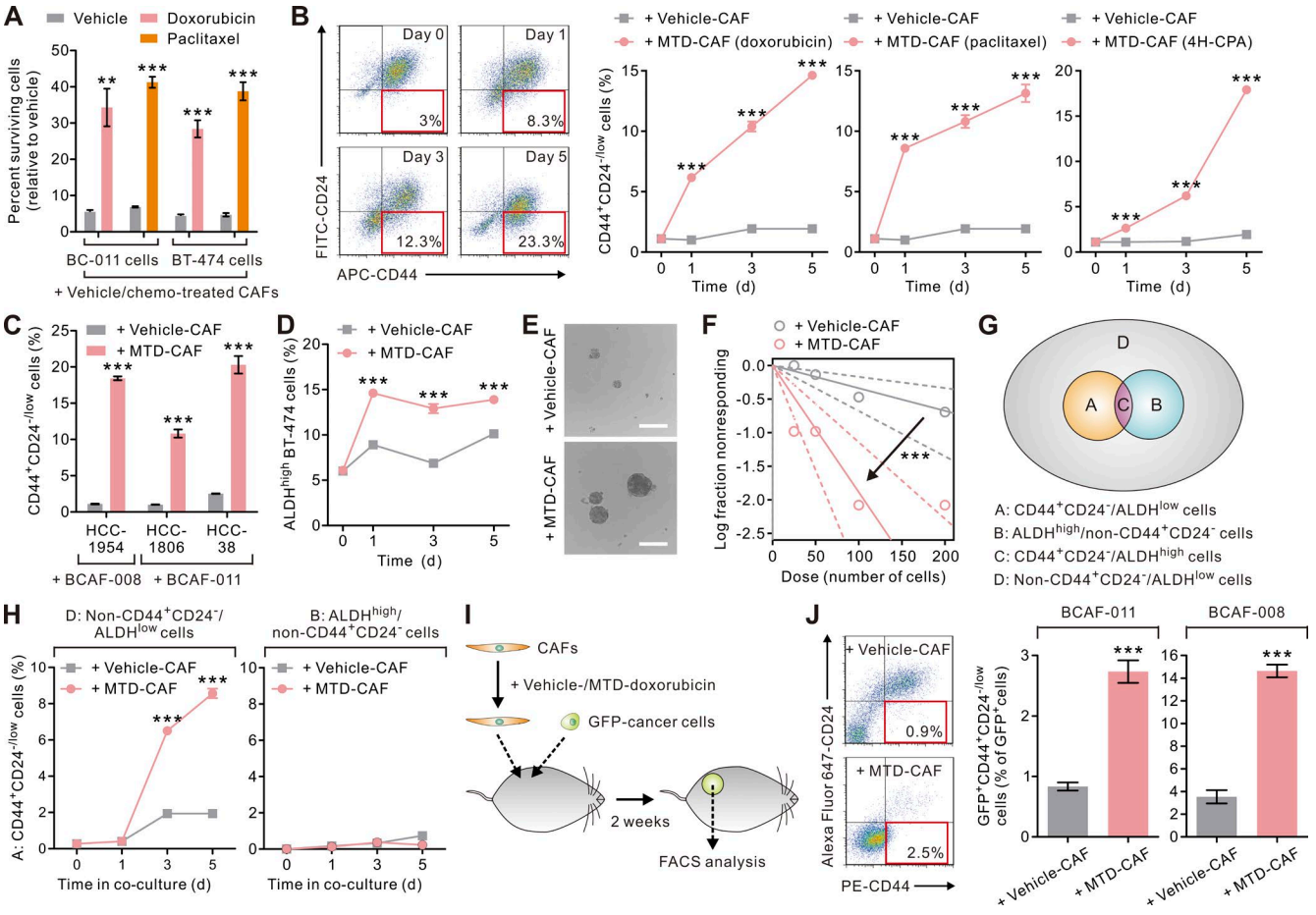

Figure 2. **MTD chemotherapy–treated CAFs increase the percentage of TICs.** (A) BCAF-011 CAFs were treated with MTD-doxorubicin, MTD-paclitaxel, or vehicle as in Fig. 1 B and then co-cultivated with BC-011 or BT-474 carcinoma cells in a dual chamber culture apparatus for 5 d, after which the carcinoma cells were isolated and treated with the same therapy regimen or vehicle for 4 d. The cells surviving the treatment were determined by a CYTOX-orange/Hoechst 33342 two-color fluorescence cell viability assay. Data from two independent experiments (n = 3 in each group) are shown. (B) BCAF-011 CAFs were treated with vehicle (vehicle-CAF), MTD-doxorubicin, MTD-paclitaxel, or MTD–4H-CPA (MTD-CAF) and then co-cultivated with BC-011 carcinoma cells in a dual chamber culture apparatus, and the carcinoma cells were subjected to flow cytometric analysis. (Left) Shown are representative plots showing patterns of CD44 and CD24 staining of carcinoma cells with the frequency of the boxed $CD44^+CD24^{-/low}$ cell population as a percentage of cancer cells shown. (Right) The percentages of $CD44^+CD24^{-/low}$ cancer cells at different times in the co-culture. Data from two independent experiments (n = 3 in each group) are shown. (C and D) The same co-culture experiments as described in B were performed using different basal (HCC-1954, HCC-1806, and HCC-38 cells; C)- or luminal (BT-474 cells; D)-subtype breast carcinoma cells and BCAF-008 (C and D) or BCAF-011 CAFs (C). Shown are the percentages of $CD44^+CD24^{-/low}$ (C) or $ALDH^{high}$ cancer cells (D) at different times in the co-culture. Data from two independent experiments (n = 3 in each group) are shown. (E) BC-011 carcinoma cells were cultured in the conditioned medium derived from vehicle- or MTD-CAFs in nonadherent culture plates for 10 d. Shown are representative phase contrast images of the resultant tumorspheres. Bars, 100 µm. (F) Limiting dilution assay demonstrating the tumorsphere formation efficiency of BC011 carcinoma cells cultured in the conditioned medium derived from vehicle- or MTD-CAFs. The arrow indicates change of slope of the trend lines, suggestive of differential tumor-sphere formation ability. Data from two independent experiments (n = 6 in each group) are shown. (G) Breast carcinoma cells can be subdivided into four subpopulations according to the expression patterns of CD44, CD24, and ALDH. (H) MTD-CAFs promoted the conversion of nonstem-like carcinoma cells (i.e., non-$CD44^+CD24^{-/low}$/$ALDH^{low}$ cells in cell subpopulation D) but not the $ALDH^{high}$ TICs (cell subpopulation B) into $CD44^+CD24^{-/low}$ cells. Data from two independent experiments (n = 3 in each group) are shown. (I) Vehicle- or MTD-doxorubicin–treated BCAF-011 or BCAF-008 CAFs were co-inoculated with GFP-transduced BC-011 and BC-008 carcinoma cells, respectively, into the mammary fat pads of NOG mice. 2 wk after cell inoculation, the tumors were removed for cell dissociation, and the cells were subjected to flow cytometric analyses. (J) The percentages of $CD44^+CD24^{-/low}$ cells relative to GFP-positive cancer cells in tumors described in I. Data from one experiment (n = 3 in each group) are shown. Data are mean ± SEM; Student's t test; **, $P < 0.01$; ***, $P < 0.001$.

MTD-CAFs produce elevated levels of ELR$^+$ chemokines

To elucidate the mechanism whereby MTD-CAFs might promote the conversion and expansion of mesenchymal-like TICs, we conducted serial transcriptomic analysis on MTD-doxorubicin– and MTD-paclitaxel–treated CAFs. Not surprisingly, we found that the pattern of gene expres-

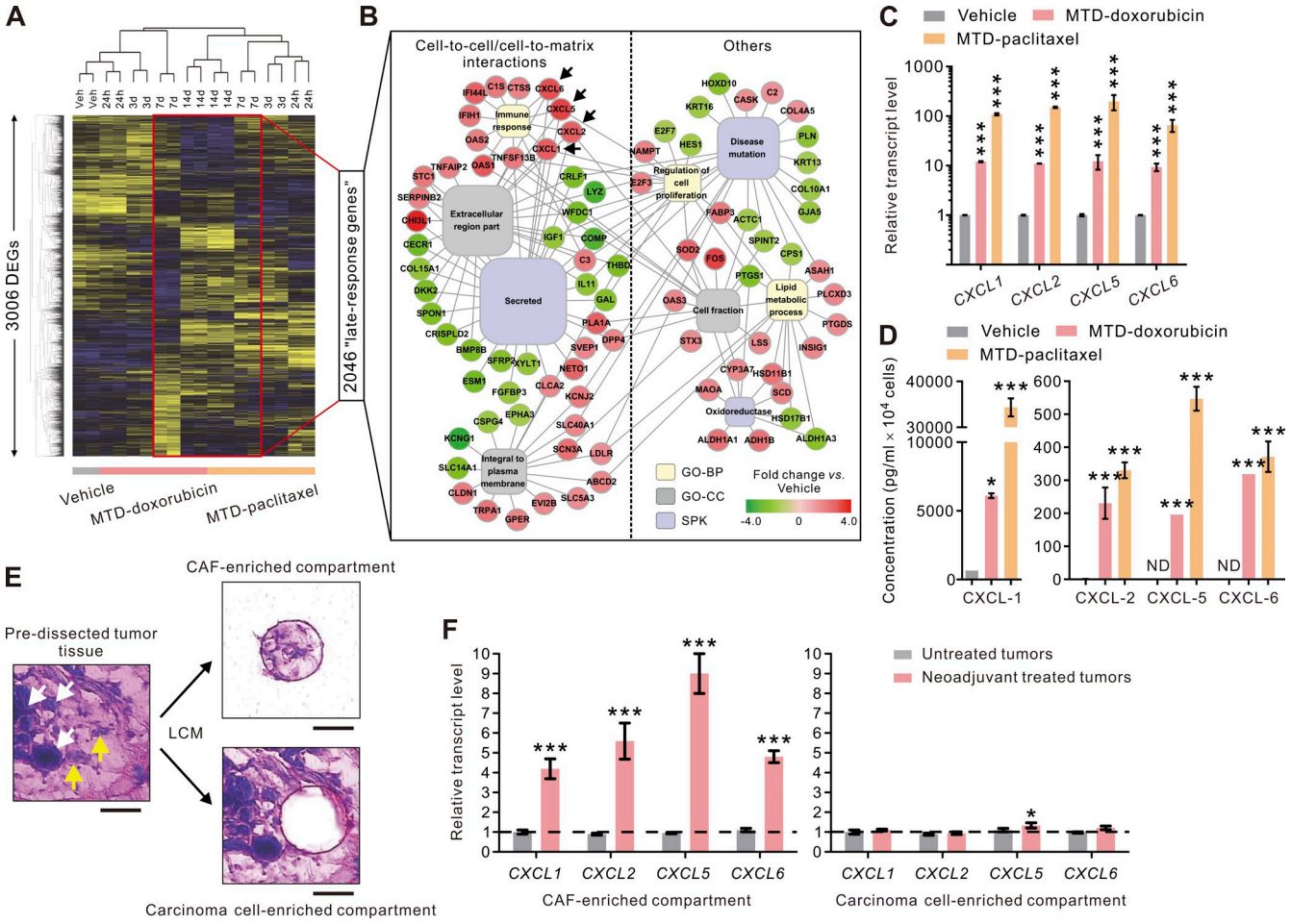

Figure 3. **MTD chemotherapy induces chronic ELR⁺ chemokine expression in CAFs.** (A) Heat map depicting hierarchical clustering of 3,006 differentially expressed genes (DEGs) detected in vehicle (Veh)-, MTD-doxorubicin–, or MTD-paclitaxel–treated BCAF-011 CAFs. The map depicts high (yellow) and low (blue) relative levels of medium-centered gene expression in log space (n = 2 at each time point). (B) Network map of enriched functional gene categories in the 2,046 late-response genes (i.e., differentially expressed genes at day 7 and/or day 14 after initiation of the treatment) detected in the chemotherapy-treated CAFs. GO-BP, gene ontology biological process; GO-CC, gene ontology cellular component; SPK, SwissProt keywords. (C) Relative transcript levels of the ELR⁺ chemokines *CXCL1*, *CXCL2*, *CXCL5*, and *CXCL6* in vehicle-, MTD-doxorubicin–, or MTD-paclitaxel–treated CAFs. Data from two independent experiments (n = 3 in each group; ***, P < 0.001) are shown. (D) The amounts of the secreted ELR⁺ chemokines detected in the conditioned medium from vehicle- and MTD-doxorubicin– or MTD-paclitaxel–treated CAFs. Data from two independent experiments (n = 3 in each group; *, P < 0.05; ***, P < 0.001) are shown. ND, not detected. (E) HistoGene-stained breast cancer tissue sections before (left) and after (right) LCM. The microdissected samples (top right) containing mainly (95%) stromal fibroblasts (yellow arrows), and those containing cancer cells were collected from the same tissue sections for subsequent RNA isolation. White arrows indicate carcinoma cells. Bars, 50 µm. (F) Relative transcript levels of the ELR⁺ chemokines measured in laser-captured tissue excised from the CAF-enriched tumor stroma (left) or the adjacent carcinoma cell–enriched region of neoadjuvant-treated or untreated human breast cancer tissues (right). At least six dissections were performed from different tumor areas from each sample. Data from three independent pairs of tumor samples (***, P < 0.001 vs. untreated tumors) are shown. Data are mean ± SEM; Student's t test.

sion changed dramatically between vehicle- and MTD-treated CAFs, and we noted that these effects became more pronounced over time (Fig. 3 A). Functional clustering analysis of a group of 2,046 differentially expressed genes in day 7 and day 14 MTD-treated CAFs identified significantly enriched gene ontology terms related to cell-to-cell and cell-to-matrix interactions (Fig. 3 B). Importantly, a survey of the up-regulated secreted factors identified four ELR motif–positive (ELR⁺) chemokines, including *CXCL1*, *CXCL2*, *CXCL5*, and *CXCL6*, as the most highly induced genes in both groups of MTD-CAFs (Fig. 3 B, arrows). Indeed, the transcript levels of these chemokines was dramatically induced by 65- to 197-fold in both groups of CAFs after MTD chemotherapy treatment (Fig. 3 C). Moreover, ELISA analysis confirmed that MTD-CAFs secreted an enormous amount of each of these ELR⁺ chemokines as compared with the vehicle-treated CAFs, which could barely produce any of them (Fig. 3 D).

The clinical relevance of the MTD-induced CAF phenotype was then verified in CAFs and epithelial tumor cells isolated by laser-capture microdissection (LCM) from neoadjuvant MTD chemotherapy–treated compared with untreated human breast cancer tissue ($n = 6$ for each; Fig. 3 E). In comparison with untreated tumors, the expression of each of the identified ELR^+ chemokines in the CAFs in the neoadjuvant-treated tumor tissue was significantly higher (Fig. 3 F, left). In contrast, there was no quantifiable difference in the expression of any of these chemokines in the epithelial tissue compartment (Fig. 3 F, right). These findings reveal that systemic MTD chemotherapy induces tissue CAFs to produce a unique profile of chemokines.

MTD-CAFs promote tumor neovascularization and macrophage infiltration and expand TICs through the ELR^+ chemokine–CXCR-2 signaling axis

Tumors with elevated levels of ELR^+ chemokines are more aggressive, and this phenotype has been attributed to their ability to stimulate angiogenesis or promote macrophage-induced immune suppression within tumors (Ali and Lazennec, 2007; Seifert et al., 2016). In addition, ELR^+ chemokines can also foster the growth and survival of stem cells (Liu et al., 2011; Jung et al., 2015). Consistently, both an in vitro angiogenesis assay and a tumor neovascularization assay revealed that the MTD-CAFs markedly promoted endothelial tube formation and tumor neovascularization, which could be efficiently blocked by SB225002, a specific inhibitor of the conserved ELR^+ chemokine receptor CXCR-2 (Fig. 4, A and B). Given the abundance of data linking chemotherapy with the infiltration of tumor-promoting TAMs (Shree et al., 2011; Bruchard et al., 2013; Hughes et al., 2015), we also considered the possibility that the recruitment of myeloid cells to tumors by chemotherapy is at least partially mediated through CAFs. Consistently, MTD-CAFs enhanced the invasiveness of macrophages in a CXCR-2–dependent manner (Fig. 4 C), and the tumors generated by co-inoculating MTD-CAFs and carcinoma cells consisted of more tumor-infiltrating TAMs, as indicated by their specific markers F4/80 and Fizz-1, than those in vehicle-CAF–containing tumors (Fig. 4 D). Importantly, in line with the prostemness functions of ELR^+ chemokines (Liu et al., 2011; Jung et al., 2015), treatment with the CXCR-2 inhibitor also reduced the level of $CD44^+CD24^{low/-}$ TICs within the breast carcinoma cells co-cultured with MTD-CAFs (Fig. 4 E). Indeed, each of the ELR^+ chemokines individually, but most especially CXCL-1 and CXCL-5, was able to significantly enhance the tumorsphere-forming ability and enhance the invasive behavior of the $CD44^+CD24^{low/-}$ TICs (Fig. 4, F and G), and each of these phenotypes could be significantly inhibited by treatment with SB225002 and/or a neutralizing antibody directed against individual chemokines (Fig. 4, H and J). These findings imply that the ELR^+ chemokines secreted by MTD-CAFs exert pleotropic tumor-promoting effects by stimulating angiogenesis and TAM recruitment and by increasing the population of TICs through CXCR-2 activation.

LDM chemotherapy attenuates ELR^+ chemokine induction in CAFs

We next sought to exploit alternative therapy regimens that could be adopted to temper the stroma response without the need for additional therapeutic intervention. In this regard, tumors treated using LDM therapy show enhanced tumor treatment response that has been attributed to reduced angiogenesis and immune modulation (Kamen, 2004; Lutsiak et al., 2005; Ghiringhelli et al., 2007; Kerbel and Tanaka et al., 2009). Given our striking findings showing that MTD-CAFs secrete enormous amounts of ELR^+ chemokines that induce angiogenesis and TAM infiltration and expand TICs, we explored the possibility that the enhanced therapy response observed after LDM therapy might be caused by a tempered CAF/ELR^+ chemokine phenotype. To test this possibility, we designed a LDM-mimetic treatment regimen in which CAFs were treated with low-dose doxorubicin (20 nM) daily for 10 consecutive days (LDM-doxorubicin) to yield an accumulative dose of the drug that was comparable with that used in the MTD regimen (Fig. 5 A). Remarkably, we observed that LDM-treated CAFs (LDM-CAFs) expressed significantly lower levels of the ELR^+ chemokines (Fig. 5 B). Similarly, paclitaxel or 4H-CPA administered to CAFs according to the LDM-mimetic regimen also failed to induce ELR^+ chemokine expression to the level observed in CAFs subjected to the same drugs using an MTD regimen (Fig. 5, C–F).

To clarify the origins for the differential ELR^+ chemokine response elicited in the CAFs, we exposed CAFs to the same total amount of doxorubicin over a protracted period of time using the different dosing regimens (Fig. 5 G). Surprisingly, we observed that when doxorubicin was administered at daily divided doses extending beyond 6 d (regimen LDM-R2), doxorubicin treatment failed to stimulate ELR^+ chemokine expression in the CAFs (Fig. 5 H), implying the blunted ELR^+ chemokine induction reflects the dosing schedule. To further explore the possibility that the LDM schedule reduced ELR^+ chemokine production by the CAFs, we lentivirally transduced BCAF-011 CAFs with GFP and inoculated them together with BC-011 carcinoma cells into the mammary fat pad of NOG mice. Once the tumors were established (2 wk after cell inoculation), we then subjected the mice to a clinically relevant MTD (2 mg/kg; roughly equivalent to the dose used in clinical regimens) or LDM-mimetic regimen of doxorubicin through systemic administration. 1 wk after cessation of treatment, the mice were sacrificed, the tumors were resected, the GFP-positive CAFs were isolated by FACS, and transcript levels of each of the four ELR^+ chemokines were quantified (Fig. 5 I). Importantly and consistent with our prediction, whereas the CAFs isolated from the MTD-doxorubicin–treated mice expressed high levels of all four ELR^+ chemokine mRNAs, the CAFs isolated from LDM-doxorubicin–treated tumors expressed comparatively low transcript levels of these same chemokines (Fig. 5 J). Thus, although an MTD treatment schedule stimulates CAFs to produce ELR^+ chemokines,

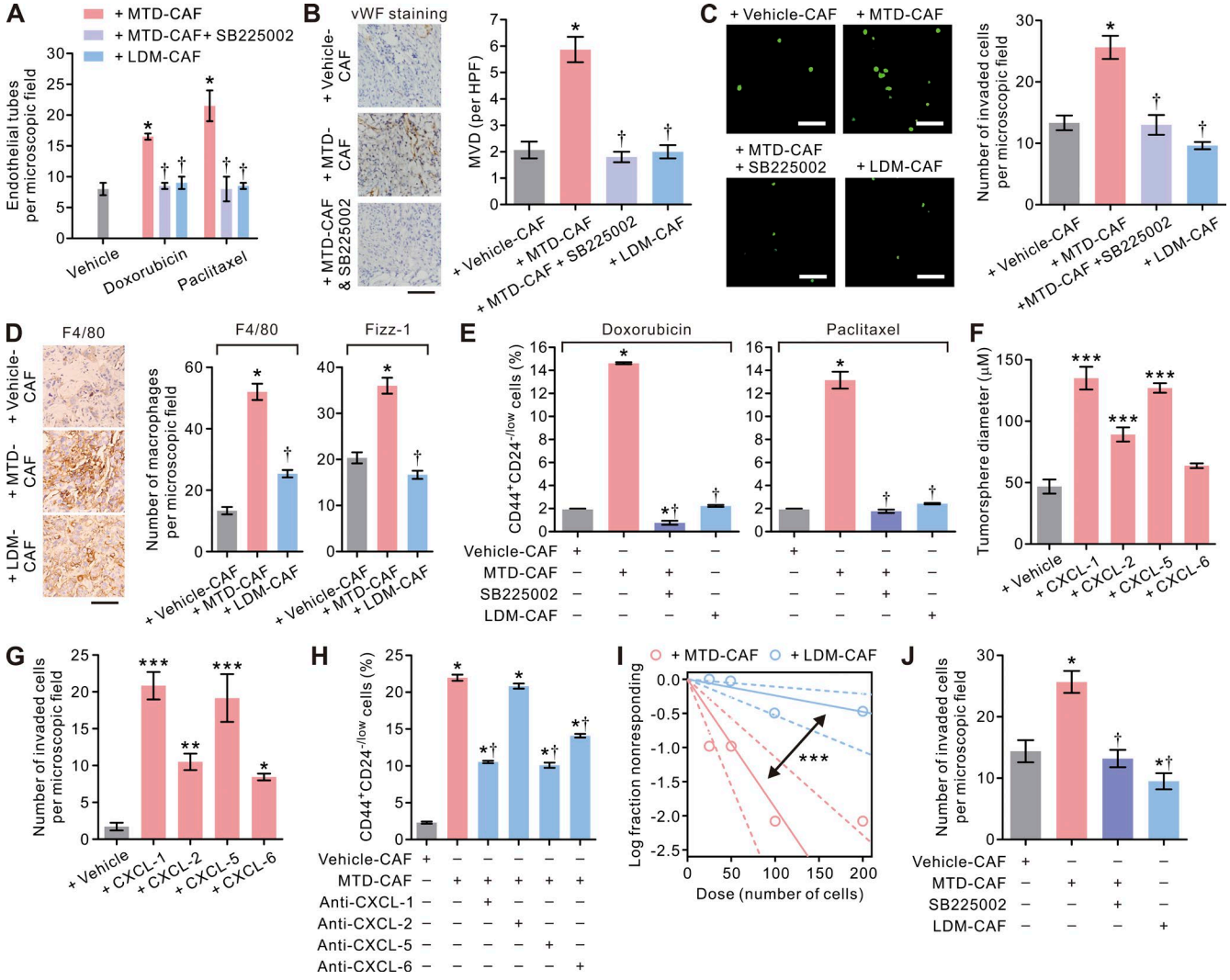

Figure 4. **The pleiotropic effects of MTD chemotherapy–treated CAFs mediated through the ELR⁺ chemokine–CXCR-2 paracrine signaling axis.** (A) Bar graphs showing the increased endothelial tube formation induced by MTD-doxorubicin– or MTD-paclitaxel–treated BCAF-011 CAFs that could be reduced by treatment with the CXCR-2 inhibitor SB225002 (1 μM) or prevented when LDM-mimetic regimens as described in Fig. 5 (A and C) were used to treat CAFs. Data from two independent experiments (n = 3 in each group) are shown. (B, left) Representative photomicrographs showing pronounced vascularity in tumors formed by orthotopically implanted BC-011 carcinoma cells along with MTD-doxorubicin (MTD-CAF)– or vehicle (vehicle-CAF)-treated CAFs with or without concurrent intraperitoneal injections of SB225002 (0.5 mg/kg/day) in NOG mice. Also shown are immunohistochemical images of von Willebrand factor (vWF) staining of the endothelial cells in the tumors. Bar, 50 μm. (Right) quantification of microvessel density (MVD) per high-power field (HPF) in tumors. At least 10 different areas were examined in each tissue. Data from one experiment (n = 3 in each group) are shown. (C, left) The invasive capacities of U937-derived macrophages in response to vehicle-CAFs, MTD-CAFs, or LDM-CAFs in the absence or presence of 1 μM SB225002 in a Transwell invasion assay. Shown are representative immunofluorescence images of the invaded cells, with cell nuclei stained with CYTOX-green. Bars, 100 μm. (Right) The numbers of invaded macrophages. Data from two independent experiments (n = 3 in each group) are shown. (D, left) Representative immunohistochemical images of F4/80 staining in tumors formed by subcutaneous inoculation of BC-011 cells along with vehicle-, MTD-, or LDM-CAFs in the flank of nude mice. Bar, 50 μm. (Right) Percent F4/80- or Fizz-1–positive cells in the microscopic field. At least 10 different areas were examined in each tissue. Data from two independent experiment (n = 3 tumor tissues in each group) are shown. (E) BCAF-011 CAFs were treated with vehicle (vehicle-CAF), MTD, (MTD-CAF), or LDM-doxorubicin or paclitaxel (LDM-CAF) as in Fig. 5 and then co-cultivated with BC-011 carcinoma cells in the presence or absence of 1 μM SB225002 in a dual chamber culture apparatus for 5 d, after which the carcinoma cells were subjected to flow cytometric analyses. Shown are the percentages of the $CD44^+CD24^{-/low}$ carcinoma cells. Data from two independent experiments (n = 3 in each group) are shown. (F) Freshly sorted $CD44^+CD24^{-/low}$ BC-011 carcinoma cells were cultured in the presence of human recombinant CXCL-1, -2, -5, and -6 (each at 1 μg/ml) or vehicle in low-attachment culture plates for 10 d, and the diameters of the tumorspheres generated were quantified. Data from two independent experiments (n = 3 in each group) are shown. (G) The ability of $CD44^+CD24^{-/low}$ BC-011 carcinoma cells to invade through reconstituted basement membrane in response to human recombinant CXCL-1, -2, -5, and -6 (each at 1 μg/ml) in a Transwell invasion assay. Data from two independent experiments (n = 3 in each group) are shown. (H) The percentages of $CD44^+CD24^{-/low}$ cells in BC-011 carcinoma cells co-cultivated with vehicle- or MTD-CAFs along with the neutralizing antibody directed against individual

this effect can be significantly blunted when an LDM treatment regimen is applied.

LDM chemotherapy prevents therapy-induced expansion of TICs

We next assessed the functional consequence of the LDM chemotherapy on the tumor phenotype. Importantly, in vitro co-culture and animal studies revealed that, as compared with the MTD-CAFs, the ability of the LDM-CAFs to promote tumor neovascularization (Fig. 4, A and B), the invasiveness of macrophages, and the tumor infiltration of TAMs (Fig. 4, C and D), to expand the population of $CD44^{+}CD24^{low/-}$ TICs (Fig. 4 E), to increase the frequencies of tumorsphere formation (Fig. 4 I), and promote the invasive phenotype (Fig. 4 J) was greatly blunted. Moreover, FACS analysis of the GFP-transduced carcinoma cells co-inoculated with CAFs into the mammary fat pads of NOG mice, which were subjected to either an MTD- or an LDM-doxorubicin regimen by intraperitoneal injection (Fig. 5 K), revealed that the percentage of $CD44^{+}CD24^{low/-}$ TICs increased substantially in the tumors from MTD-doxorubicin–treated mice but did not in the LDM-doxorubicin–treated mice (Fig. 5 L). These findings argue that the improved patient response observed after an LDM-chemotherapy treatment regimen likely reflects a tempering of CAF activation characterized by reduced ELR^{+} chemokine induction and a consequent reduction in TIC expansion and tumor aggression.

LDM chemotherapy attenuates therapy-triggered STAT-1/NF-κB–ELR^{+} chemokine signaling in CAFs

To clarify why MTD treatment induces such a profound stromal fibroblast activation, we conducted bioinformatics knowledge-based analysis on the promoters of the up-regulated ELR^{+} chemokines. Our experiments revealed that each of these chemokine promoters harbored an enrichment for STAT-1 and nuclear factor κ light-chain enhancer of activated B cells (NF-κB) binding motifs (Fig. 6 A). In line with this prediction, immunoblot analysis revealed that only MTD-treated but not LDM-treated CAFs had elevated levels of phosphorylated STAT-1 (p–STAT-1) as well as an increased ratio between the phosphorylated form and the total abundance of the NF-κB inhibitor protein I-κBα (I-κBα; Fig. 6, B and C), and luciferase reporter assays revealed heightened STAT-1 and NF-κB transcriptional activities in MTD-treated CAFs but much less in LDM-treated CAFs (Fig. 6 D). Consistently, immunohistochemical analyses confirmed that the p–STAT-1–positive, activated CAFs were abundantly present in the stroma of MTD-doxorubicin–treated tumors but much less so in LDM-therapy–treated tumors (Fig. 6 E). A functional link between elevated STAT-1 and NF-κB activity and ELR^{+} chemokine production in the MTD-CAFs was further demonstrated by showing that BCAF-011 CAFs lentivirally transduced with a phosphorylation-deficient mutant of STAT-1 or IκBα were unable to up-regulate expression of any of the ELR^{+} chemokines after MTD treatment (Fig. 6 F). Moreover, loss of STAT-1 and NF-κB activity in the MTD-CAFs inhibited their ability to expand the population of $CD44^{+}CD24^{low/-}$ TICs within the parental breast cancer cell population (Fig. 6 G). These data suggest that MTD chemotherapy treatment activates STAT-1 and NF-κB in CAFs, which thereafter induces ELR^{+} chemokine expression that, once secreted, fosters the transdifferentiation and expansion of TICs. This phenotype is prevented using a LDM treatment regimen and, consequently, so too is the enrichment for TICs.

LDM chemotherapy enhances treatment response in desmoplastic breast cancer

Given our finding that LDM chemotherapy tempers CAF activation and TIC expansion, we next asked whether an LDM regimen would reduce tumor aggression and enhance treatment response. To begin with, we noted that the orthotopic tumors developed in mice co-injected with BC-011 carcinoma cells, and LDM-CAFs not only grew considerably slower than the tumor cells co-inoculated with MTD-CAFs, but we also detected fewer lymph nodes and distant metastatic tumors (Fig. 7 A and not depicted). To determine whether these phenotypes could be replicated after in vivo chemotherapy, we first confirmed that the clinically relevant MTD- and LDM-mimetic doxorubicin therapy (Fig. 5 A) both were able to efficiently kill most (>90%) of the carcinoma cells in vitro (Fig. 7 B), based on which we devised MTD- and LDM-mimetic chemotherapy regimens that mimicked the cyclic systemic treatment of breast cancer patients (Fig. 7 C). We first sought to directly investigate the effect of systemic chemotherapy–treated CAFs on tumor cells by stably infected HCC-1954 carcinoma cells (derived from a patient with a basal-subtype primary breast cancer) with the antiapoptotic protein Bcl-2, which rendered them apoptotic and treatment resistant (not depicted), and co-inoculated them with BC-011 CAFs into the flanks of nude mice. The mice then received cyclic injections of either vehicle or doxorubicin using either the MTD- or the LDM-mimetic regimen. Consistent with our earlier findings, we noted that the chemo-resistant BCL-2–expressing tumors in the mice treated with the MTD

ELR^{+} chemokines. Data from two independent experiments ($n = 3$ in each group) are shown. (I) Limiting dilution assay demonstrating the tumorsphere formation efficiency of BC-011 carcinoma cells cultured in the conditioned medium from MTD- or LDM-CAFs. The arrow indicates change of slope of the trend line, suggestive of differential tumorsphere formation ability. Data from one experiment ($n = 6$ in each group; mean ± SEM; Student's *t* test; ***, $P < 0.001$ vs. MTD) are shown. (J) The invasive capacities of BC-011 cells in response to vehicle-, MTD-, or LDM-CAFs, with or without 1 µM SB225002, in a Transwell invasion assay. Shown are the numbers of the invaded cancer cells per microscopic field. Data from two independent experiments ($n = 3$ in each group) are shown. (A–H and J) Data are mean ± SEM; Student's *t* test; *, $P < 0.05$; **, $P < 0.01$; ***, $P < 0.001$ versus vehicle. †, $P < 0.05$ versus MTD.

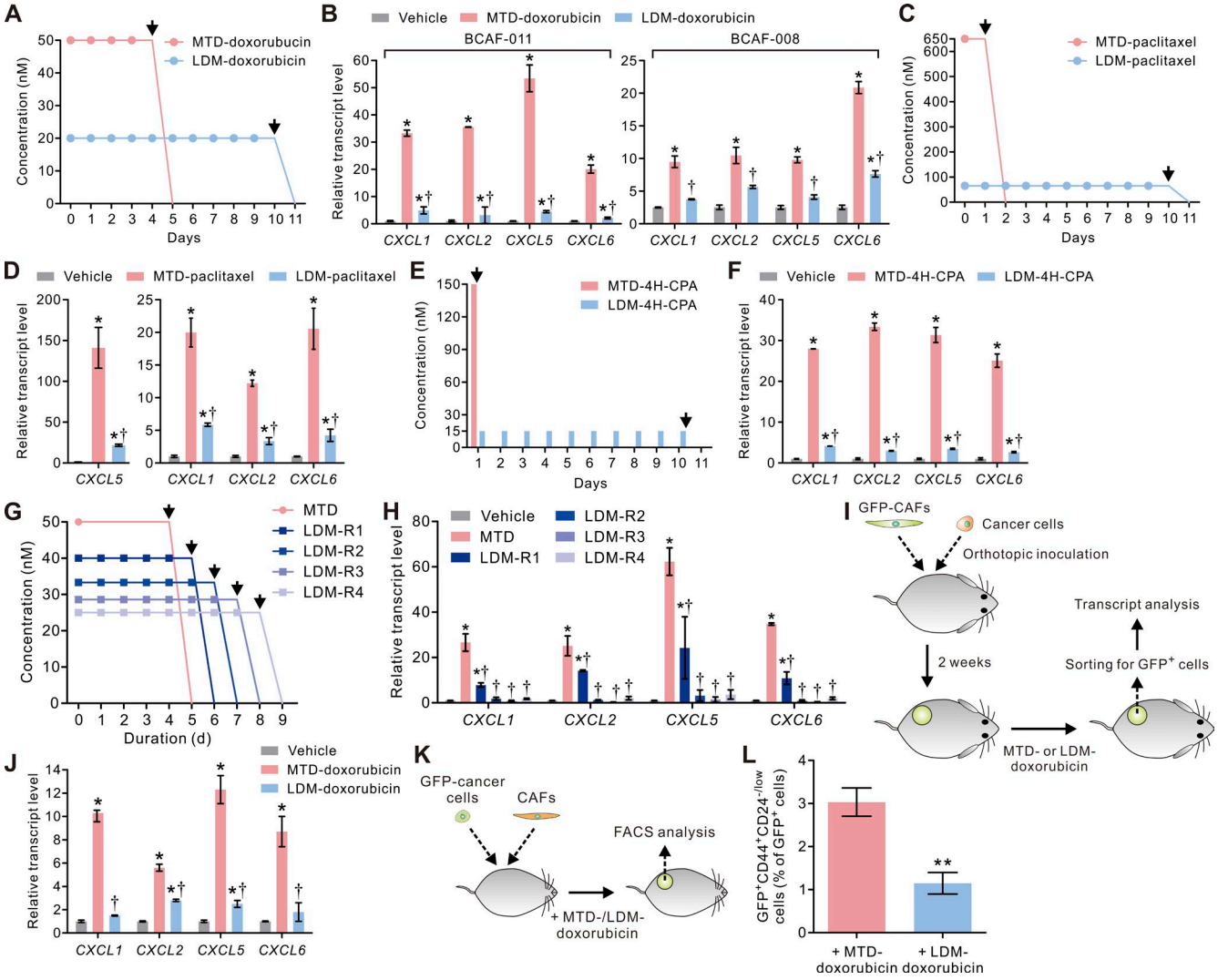

Figure 5. **LDM chemotherapy attenuates the treatment-induced expressions of ELR⁺ chemokines in CAFs.** (A) Schematic showing doxorubicin treatment protocols that mimic MTD and LDM chemotherapy regimens. (B) The transcript levels of the ELR⁺ chemokines *CXCL1*, *CXCL2*, *CXCL5*, and *CXCL6* in vehicle, MTD-doxorubicin–, or LDM-doxorubicin–treated BCAF-011 or BC-008 CAFs 14 d after initiation of the treatments. Data from two independent experiments ($n = 3$ in each group) are shown. (C) Schematic showing paclitaxel treatment protocols that mimic MTD (650 nM × 24 h) and LDM (65 nM daily × 10 d) chemotherapy regimens ($n = 3$ in each group). (D) The transcript levels of the ELR⁺ chemokines in vehicle-, MTD-paclitaxel–, or LDM-paclitaxel–treated BCAF-011 CAFs 14 d after initiation of the treatments. Data from three independent experiments ($n = 3$ in each group) are shown. (E) Schematic showing 4H-CPA treatment protocols that mimic MTD (150 nM × 1 h) and LDM (15 nM × 1 h daily for 10 d) chemotherapy regimens. (F) The transcript levels of the ELR⁺ chemokines in vehicle, MTD–4H-CPA–, or LDM–4H-CPA–treated BCAF-011 CAFs 14 d after initiation of the treatments. Data from three independent experiments ($n = 3$ in each group) are shown. (G) Schematic showing doxorubicin treatment protocols that recapitulate MTD (50 nM X 96 h)- or different LDM-mimetic regimens with gradually prolonged lengths of drug exposure (from LDM-R1 to LDM-R4). Note that the total accumulated doses of drug exposure, as reflected in area under curves, were the same across all the treatment groups (4,800 nM × h). (A, C, E, and G) Arrows indicate time of drug clearance by wash. (H) Fold-increases in the transcript levels of the ELR⁺-chemokines in BCAF-011 CAFs exposed to vehicle or doxorubicin using the treatment protocols described in G. Data from three independent experiments ($n = 3$ in each group) are shown. (I) BCAF-011 CAFs were lentivirally infected with GFP and then co-injected with BC-011 carcinoma cells into the mammary fat pads of NOG mice. 2 wk after cell inoculation, the tumors were given injections of vehicle or doxorubicin at an MTD (2 mg/kg as a single-dose intravenous injection)- or an LDM (0.2 mg/kg every day by intraperitoneal injections for 10 consecutive days)-mimetic therapy regimen and then removed for cell dissociation followed by transcript analyses. (J) The transcript levels of the ELR⁺ chemokines in the GFP⁺ CAFs isolated from the tumors in I. Data from one experiment ($n = 5$ in each group) are shown. (K) BCAF-011 CAFs were co-inoculated with GFP-transduced BC-011 carcinoma cells into the mammary fat pads of NOG mice. The resultant tumors were given injections of vehicle or doxorubicin at a MTD- or a LDM-mimetic regimen as described in I. The tumors were then removed for cell dissociation followed by flow cytometric analyses. (L) The percentages of $GFP^+CD44^+CD24^{-/low}$ cells relative to the GFP⁺ carcinoma cells isolated from the tumors described in K. Data from one experiment ($n = 5$ in each group) are shown. Data are mean ± SEM; Student's *t* test. *, $P < 0.05$; **, $P < 0.01$ versus vehicle. †, $P < 0.05$ versus MTD.

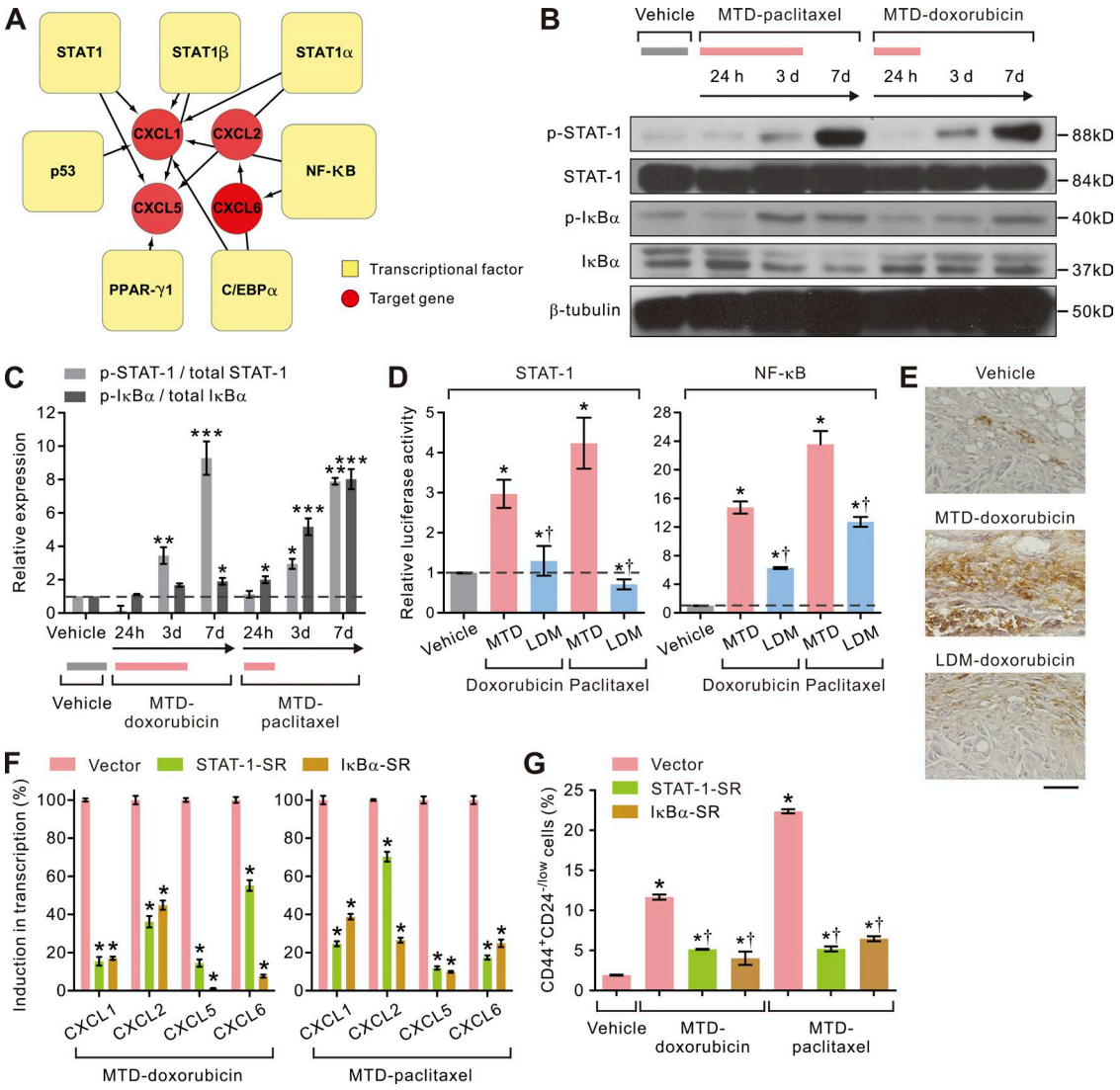

Figure 6. **LDM chemotherapy tempers STAT-1– and NF-κB–dependent ELR⁺ chemokine expressions in CAFs.** (A) Schematic showing enrichment for STAT-1, NF-κB, PPAR-γ, C/EBP-α, and p53 binding sites in the promoters of the ELR⁺ chemokines highly induced in MTD chemotherapy–treated BCAF-011 CAFs. (B) Representative immunoblots showing sustained activation of STAT-1 (p-STAT-1) and IκBα (p-IκBα) in vehicle-, MTD-doxorubicin–, or MTD-paclitaxel–treated BCAF-011 CAFs. β-tubulin was included as a loading control. (C) Bar graphs quantifying immunoblot data shown in B. Data from two independent experiments (*, $P < 0.05$; **, $P < 0.01$; ***, $P < 0.001$ vs. vehicle) are shown. (D) Bar graphs quantifying fold STAT-1– and NF-κB–mediated luciferase expression in MTD- or LDM-treated BCAF-011 CAFs relative to vehicle-treated control. Data from three independent experiments ($n = 3$ in each group. *, $P < 0.05$ vs. vehicle; †, $P < 0.05$ vs. MTD) are shown. (E) Representative immunohistochemical images of p-STAT-1 staining in vehicle-, MTD-doxorubicin– , or LDM-doxorubicin–treated desmoplastic tumors generated by co-inoculating BC-011 cells and BCAF-011 CAFs into the mammary fat pads of NOG mice. Bar, 100 µm. (F) The transcript levels of the ELR⁺ chemokines induced after MTD-doxorubicin or MTD-paclitaxel treatment in vector-transduced BCAF-011 CAFs or those lentivirally transduced with a STAT-1–SR– or an IκBα-SR–expressing vector to inhibit the STAT-1 and NF-κB activity, respectively. Data from three independent experiments ($n = 3$ in each group. *, $P < 0.05$ vs. vector) are shown. (G) Vector-, STAT-1– SR–, or IκBα-SR–transduced BCAF-011 CAFs were treated with MTD-doxorubicin, MTD-paclitaxel, or vehicle and then co-cultivated with BC-011 carcinoma cells in a dual chamber culture apparatus for 5 d, after which the carcinoma cells were subjected to flow cytometric analyses. Shown are percentages of $CD44^{+}CD24^{-/low}$ cell subpopulation in each group. Data from three independent experiments ($n = 3$ in each group. *, $P < 0.05$ vs. vehicle-CAF; †, $P < 0.05$ vs. vector-transduced CAF) are shown. Data are mean ± SEM; Student's *t* test.

chemotherapy protocol grew significantly faster than either the vehicle-treated mice or the mice subjected to a LDM therapy regimen (Fig. 7 D). In a second model wherein the mammary fat pads of NOG mice were co-inoculated with control and apoptotic-sensitive HCC-1954 cells and primary CAFs, single-agent therapy with LDM-doxorubicin could profoundly inhibit the growth of the tumors, and its treatment efficacy was comparable with that in those con-

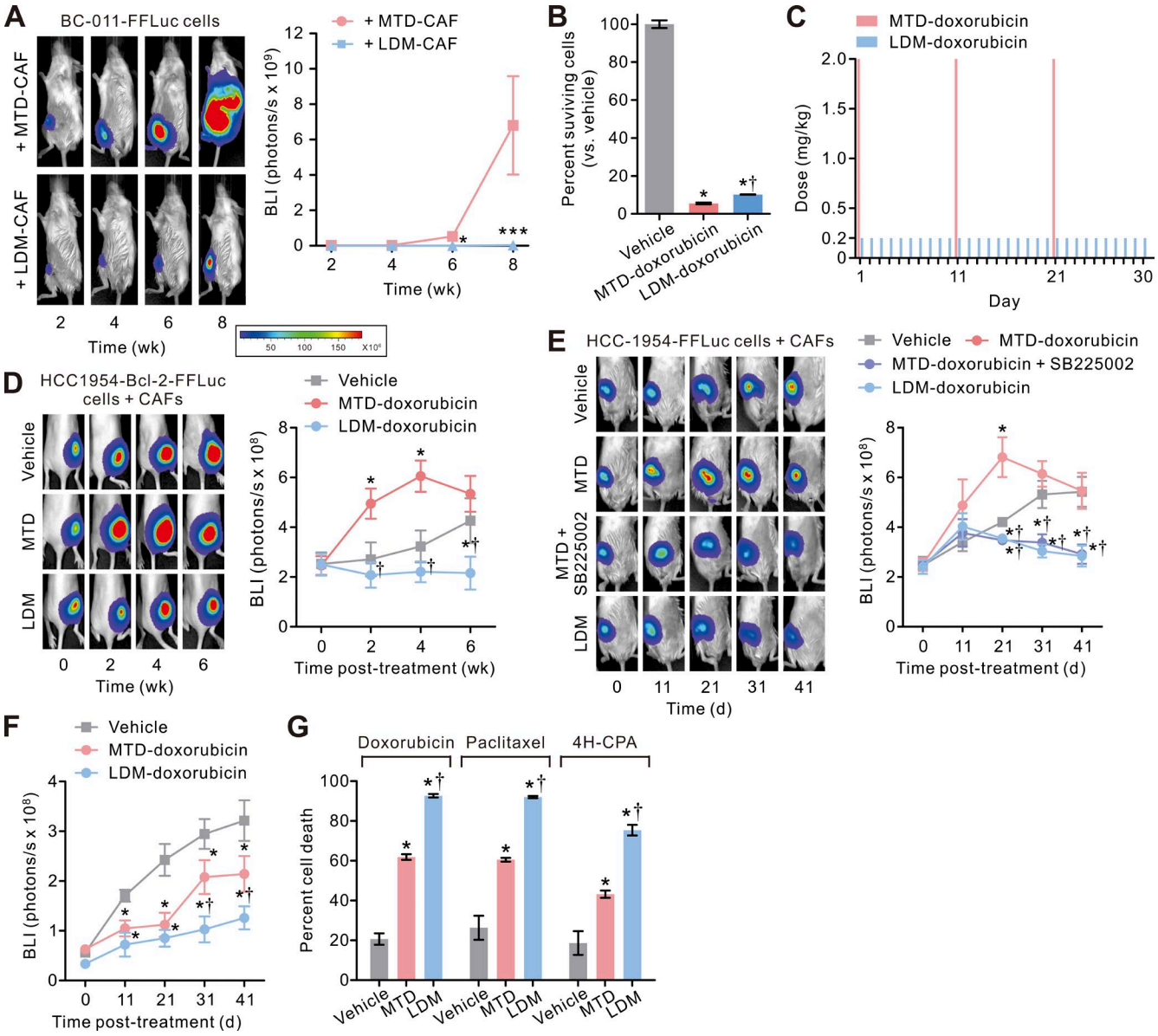

Figure 7. **LDM chemotherapy enhances treatment response and prevents TIC expansion in desmoplastic breast cancer.** (A, left) BCAF-011 CAFs were treated with MTD (MTD-CAF) or LDM-doxorubicin (LDM-CAF) as in Fig. 5 A and then co-injected with FFLuc-transduced BC-011 carcinoma cells into the mammary fat pads of NOG mice. Tumor bulk was then monitored using BLI. Shown is representative BLI of tumors at the indicated time after cell inoculation. (Right) Tumor bulk quantified as BLI normalized photon counts as a function of time. Data from one experiment ($n = 6$ in each group; mean ± SEM; Student's t test; *, $P < 0.05$; ***, $P < 0.001$ vs. MTD-CAF) are shown. (B) HCC-1954 carcinoma cells were treated with vehicle or doxorubicin using an MTD- or an LDM-mimetic regimen as described in Fig. 5 A, and the cells surviving the therapy were determined by CYTOX-orange/Hoechst 33342 two-color fluorescence cell viability assay 10 d after initiation of the treatments. Data from three independent experiments ($n = 3$ in each group) are shown. (C) Schematic showing in vivo doxorubicin treatment protocols that mimic MTD and LDM chemotherapy regimens. The tumor-bearing mice received cyclic (three cycles) injections of vehicle or doxorubicin using an MTD (2 mg/kg by intravenous injections every 10 d for three cycles)- or an LDM (0.2 mg/kg by intraperitoneal injections daily for 30 d)-mimetic regimen. (D) BCAF-011 CAFs were co-inoculated with Bcl-2–transduced HCC-1954 carcinoma cells subcutaneously into the flanks of nude mice. 2 wk later, the tumor-bearing mice received cyclic intraperitoneal injections of vehicle or doxorubicin using the MTD- or LDM-mimetic regimen as described in C. (Left) Shown are representative bioluminescence images of tumors at the indicated time after initiation of the therapy. (Right) Tumor bulk quantified as BLI normalized photon counts as a function of time. Data from one experiment ($n = 6$ in each group) are shown. (E) BCAF-011 CAFs were co-inoculated with FFLuc-transduced HCC-1954 carcinoma cells into the mammary fat pads of NOG mice, and the resultant tumors were treated as in C with or without concurrent intraperitoneal injections of SB225002 (0.5 mg/kg/day) in the mice. (Right) Tumor bulk plotted over time. Data from one experiment ($n = 6$ in each group) are shown. (F) FFLuc-transduced HCC-1954 carcinoma cells were inoculated into the mammary fat pads of NOG mice without co-inoculation of CAFs. The resultant pauci-CAF tumors were treated as in C, and the tumor bulk was plotted over time. Data

currently treated with MTD therapy and the CXCR-2 inhibitor (Fig. 7 E). Notably, the desmoplastic tumors treated with the MTD-mimetic regimen outgrew the control tumors during the initial period of the treatment (day 0 to day 31 in Fig. 7 E), whereas the same MTD therapy significantly suppressed the growth of the tumors generated when only the carcinoma cells without CAFs were inoculated into the mice despite that these pauci-CAF tumors grew much more slowly than the desmoplastic tumors (Fig. 7 F). This result raised the intriguing possibility that the tumor-promoting effects of the chemo-treated CAFs may override the cytotoxic and antitumor effect of traditional MTD chemotherapy in certain stroma cell–abundant desmoplastic tumors. We also verified that the higher antitumor efficacy of LDM therapy than MTD therapy was not drug specific, as it was also evident when the cancer cell/CAF co-culture was treated with other types of chemotherapy agents such as paclitaxel and 4H-CPA (Fig. 7 G).

To validate that LDM therapy indeed imparts therapeutic benefits in a more clinically relevant paradigm, we repeated the in vivo animal studies using highly aggressive breast cancer MDA-MB-436 cells in CD34 hematopoietic stem cell (HSC)–reconstituted humanized NOG (HSC-hu-NOG) mice, which contain functionally differentiated human immune cells. We found that the tumors in this humanized mouse model of orthotopic and desmoplastic breast cancer responded to LDM therapy but not to standard MTD chemotherapy so that the LDM therapy–treated mice survived significantly longer than those subjected to standard chemotherapy (Fig. 8, A and B), supporting that LDM therapy indeed conferred survival benefits to tumor-bearing mice. In addition, flow cytometric analyses of the resulting tumors revealed that the mice treated with standard MTD chemotherapy had a greater number of $CD44^+CD24^{low/-}$ TICs as compared with those administered the LDM therapy regimen or co-administered with the CXCR-2 inhibitor (Fig. 8, C and D). Because these phenotypes were not observed in tumors generated in mice orthotopically injected with the carcinoma cells alone (Fig. 8, E and F), these findings support our notion that chemotherapy treatment can drive tumor aggression and treatment resistance by activating stromal fibroblasts. Next, as mouse xenografts of human cancer cells do not necessarily recapitulate the tissue architecture and the microenvironment of human tumors and may lack predictive value with regard to chemotherapy treatment response and the rate of tumor progression (Hidalgo et al., 2014), we repeated the experiments in a highly clinically relevant patient-derived xenografted (PDX) mouse breast tumor model. We first confirmed that these PDX tumors had a considerable stromal content with ∼25–30% α-SMA–positive stromal fibroblasts per microscopic field (Fig. 8 G). Consistently, single-agent chemotherapy using the LDM-doxorubicin regimen substantially reduced the growth rate of the tumors in this model, whereas MTD therapy only slightly inhibited the tumor growth (Fig. 8, H and I). Furthermore, flow cytometric analyses on the breast cancer cells isolated from these PDX tumors using a specific marker of human breast cancer cells CD298 (Lawson et al., 2015) confirmed that the PDX tumors treated with LDM therapy contained significantly less $CD44^+CD24^{low/-}$ TICs than those treated with MTD therapy (Fig. 8 J and Fig. S2).

LDM chemotherapy enhances treatment response in desmoplastic PDAC

Having demonstrated the beneficial effect of LDM chemotherapy in desmoplastic breast cancer, we asked whether this phenomenon was not confined only to breast cancer–CAF interactions, but also could be extended to other types of desmoplastic cancers such as PDAC (Sherman et al., 2014). It has been shown that LDM chemotherapy can attenuate therapy-induced metastasis caused by rebound MDSC mobilization and increased angiogenesis in PDAC (Hasnis et al., 2014). We therefore sought to compare the impact of an LDM versus an MTD chemotherapy routine on PDAC cells–pancreatic stellate cell (PSC; the most abundant fibroblast-like stromal cells in PDAC) interactions. We treated PSCs with either a clinically relevant MTD (20 μM × 30 min; Grunewald et al., 1992) or an LDM-mimetic (2 μM × 30 min for 10 consecutive days; Fig. 9 A) regimen using the standard of care PDAC chemotherapy drug gemcitabine and assayed transcript levels of ELR^+ chemokines in the PSCs. Consistent with our findings in breast CAFs, we found that PSCs treated with MTD-gemcitabine (MTD-PSCs) expressed high levels of all four ELR^+ chemokines, whereas those subjected to an LDM regimen (LDM-PSCs) expressed much lower levels of those chemokines (Fig. 9 B). Furthermore, FACS analysis of PANC-1 cells or primary SP-1 PDAC cells co-cultured with MTD-PSCs revealed that these cells contained a progressively increasing percentage of $CD44^+CD133^+$ cells or $CD44^+CD24^+$ cells (Fig. 9, C–F; and Figs. S3 and S4), which we and others have previously shown to contain TICs in PDAC (Li et al., 2007; Wang et al., 2013), whereas the cells co-cultured with LDM-PSCs had a lower percentage of TICs.

In accordance with the findings in breast cancer, parallel studies using FFLuc-transduced PANC-1 PDAC cells co-injected orthotopically into the pancreas with MTD-PSCs in HSC-hu-NOG mice grew dramatically faster than those co-injected with LDM-PSCs. Moreover, the PANC-1 PDAC

from one experiment (n = 6 in each group) are shown. (G) HCC-1954 carcinoma cells were co-cultivated with BCAF-011 CAFs in a dual-chamber culture apparatus, and the co-cultures were treated with doxorubicin, paclitaxel, or 4H-CPA using the various MTD- or LDM-mimetic regimens for one treatment cycle as described in Fig. 5. The cells surviving the treatment were determined as in B. Data from three independent experiments (n = 3 in each group) are shown. (B and D–G) Data are mean ± SEM; Student's t test. *, $P < 0.05$ vs. vehicle. †, $P < 0.05$ vs. MTD.

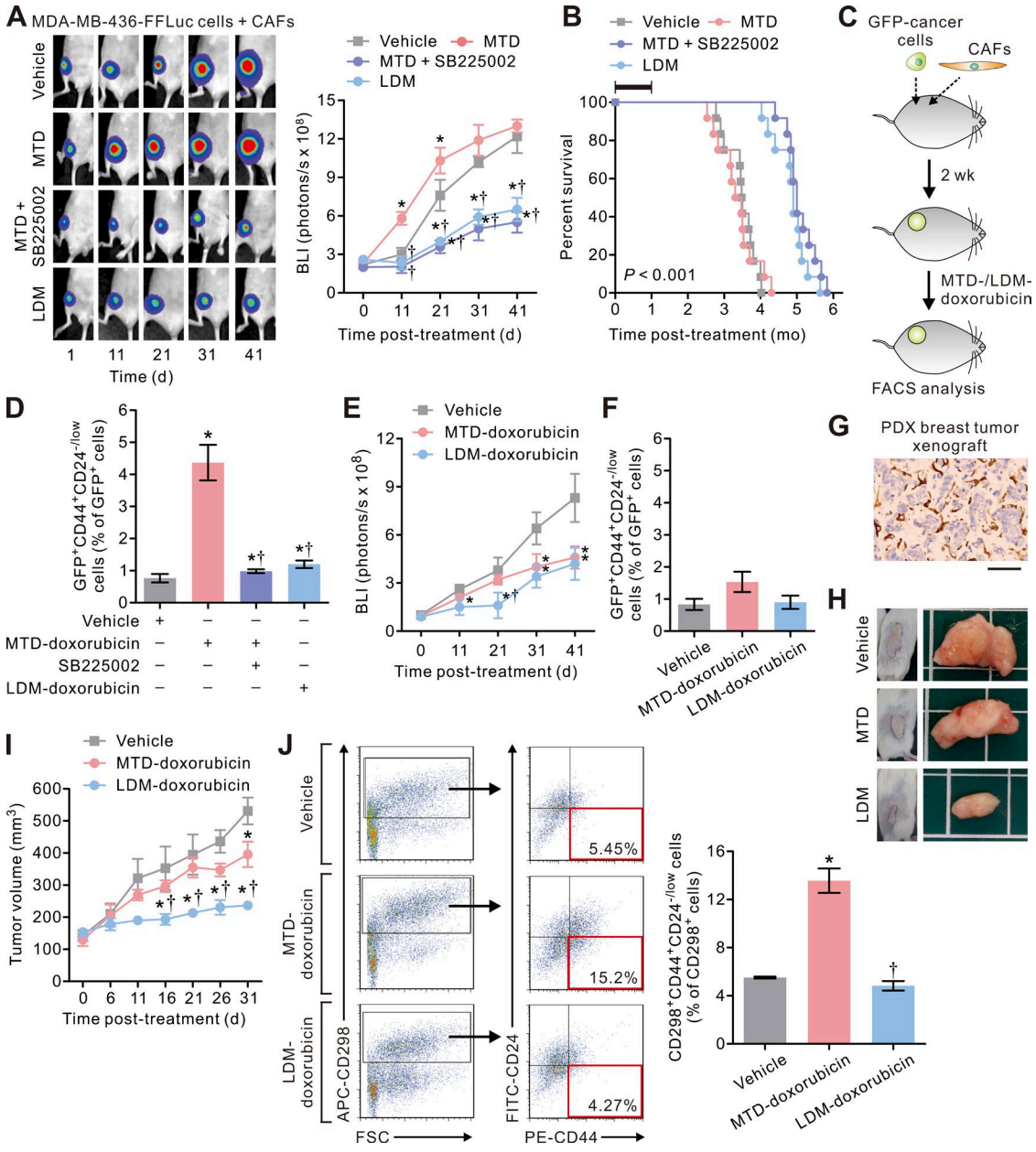

Figure 8. **LDM chemotherapy enhances treatment response in humanized or PDX mouse breast cancer models.** (A, left) BCAF-011 CAFs were co-inoculated with GFP-FFLuc–transduced MDA-MB-436 carcinoma cells into the mammary fat pads of humanized HSC-hu-NOG mice, and the resultant tumors were treated as in Fig. 7 C with or without concurrent intraperitoneal injections of SB225002 (0.5 mg/kg/d) in the mice. (Right) Tumor bulk plotted over time. Data from one experiment (n = 10 in each group) are shown. (B) Percent survival as a function of time in mice described in A. The black bar indicates the duration of treatment. Data from one experiment (n = 10 in each group; the survival curves were compared using log-rank test; LDM vs. MTD) are shown. (C and D) After the first cycle of chemotherapy in A, the tumors were removed for cell dissociation followed by flow cytometric analyses. (D) Shown are the percentages of $CD44^+CD24^{-/low}$ cells relative to the GFP^+ carcinoma cells. Data from two independent experiments (n = 3 in each group) are shown. (E) MDA-MB-436 carcinoma cells were inoculated into the mammary fat pads of HSC-hu-NOG mice without co-inoculation of CAFs. The resultant pauci-CAF tumors were treated as in A, and the tumor bulk was plotted over time. Data from one experiment (n = 6 in each group) are shown. (F) The percentages of $CD44^+CD24^{-/low}$ cells relative to the GFP^+ carcinoma cells isolated from the tumors generated in E. Data from two independent experiments (n = 3 in each group) are shown. (G) Representative immunohistochemical images of α-SMA staining in a PDX breast tumor xenograft. Bar, 100 µm. (H) NOD-SCID γ mice bearing PDX breast tumors were treated with systemic MTD- or LDM-doxorubicin as in Fig. 7 C, and the tumor growth was monitored for 31 d after initiation of the treatments. Shown are representative photographs of the tumors in each group at the study end point. (I) Tumor volume in H plotted over time. Data from one experiment (n = 6 in each group) are shown. (J) The PDX tumors as described in I were removed for cell dissociation followed by flow cytometric analyses after the first treatment cycle (i.e., 11 d after initiation of the treatments). (Left) Shown are representative plots showing patterns of

cells co-injected with the MTD-PSCs rapidly and extensively developed liver, peritoneum, and lung metastasis (Fig. 9 G and not depicted). Indeed, whereas a systemic MTD-mimetic regimen of gemcitabine treatment (Fig. 9 H) fostered the growth and dissemination of orthotopically implanted PANC-1 pancreatic tumors co-injected with PSCs, those same mice treated with an LDM-mimetic regimen survived longer, and their tumors regressed significantly (Fig. 9, I and J).

Collectively, these findings argue that a standard of care MTD chemotherapy regimen activates STAT-1 and NF-κB in stromal fibroblasts to induce ELR^+ chemokine expression that then drives tumor aggression and treatment resistance, at least in part by stimulating tumor neovascularization and the infiltration of TAMs and by fostering the transdifferentiation of carcinoma cells and the expansion of TICs (Fig. 10 A). Our results also demonstrate that these effects can be largely tempered by adopting an LDM treatment approach and that the phenotype is not confined to one tumor type but is likely universal in nature (Fig. 10 B).

DISCUSSION

In this study, we presented compelling evidence demonstrating that MTD chemotherapy used to treat human cancers can exert sustained effects on the tumor stroma that include the induction of an ELR^+ chemokine–producing phenotype in CAFs, whereby they can subsequently promote tumor aggression. Our data revealed that ELR^+ chemokine–producing CAFs are abundant and readily detected in cancer tissues, even after multiple cycles of therapy. We further determined that MTD chemotherapy induces a population of CXCR-2–dependent TICs through inducing the CAF ELR^+ chemokine–cancer cell paracrine signaling process, which can be much tempered by switching to LDM therapy regimens. Thus, our findings emphasize the crucial contribution of the tissue stroma in cancer treatment and imply that LDM chemotherapy may provide a new avenue for preventing stromal activation to further enhance the therapeutic outcome in desmoplastic cancers.

It is increasingly recognized that systemic chemotherapy can activate the tumor stroma to modulate tumor behaviors in human cancers. In human prostate cancer, the genotoxic agent mitoxantrone was able to stimulate Wnt16B secretion by stromal fibroblasts, which then promoted the proliferation and invasion of the associated carcinoma cells (Sun et al., 2012). In human colorectal cancer, chemotherapy led to the enrichment of IL-17A–producing CAFs within the tumor stroma, which in turn promoted the self-renewal of TICs and tumor growth (Lotti et al., 2013). Echoing these findings, our study showed that, after chemotherapy treatment, breast cancer CAFs chronically up-regulate several factors linked to cell-to-cell and/or cell-to-matrix interactions. Our mechanistic studies additionally dissect the functional alterations in chemo-treated CAFs. An unbiased expression profiling, followed by comprehensive bioinformatics analyses and molecular and functional studies, led to the identification of the ELR^+ chemokine–CXCR-2 paracrine signaling process, stimulated by chronically elevated STAT-1 and NF-κB transcriptional activity in CAFs, as an essential mechanism underlying the pro-oncogenic and pro-TIC activities of chemo-treated CAFs. Furthermore, and importantly, we demonstrated the clinical significance of this finding by showing that there is a significant induction of the ELR chemokines in the stroma of neoadjuvant chemotherapy–treated human cancer tissues. It is worth noting that the expressions of several previously reported CAF-derived factors, including CXCL12 (SDF-1α), G-CSF, and VEGF-A (Orimo et al., 2005; McAllister and Weinberg, 2014), were not significantly induced by MTD chemotherapy in CAFs (unpublished data). This indicates that the chemotherapy-elicited stroma alterations are mediated by signaling pathways distinct from those functioning in incipient or chemo-naive tumors.

To date, several clinical trials have supported LDM chemotherapy alone or in combination with targeted therapeutics or antiangiogenic drugs as an effective approach in cancer treatment (Pasquier et al., 2010; Loven et al., 2013). For instance, in patients with breast cancer, it has been estimated that LDM therapy yielded an average response rate of 39% and an average overall clinical benefit of 57%. Recently, a large and randomized phase III trial, the CAIRO3 trial, provided a solid support for the clinical benefits of LDM chemotherapy in metastatic colorectal cancer (Kerbel and Grothey, 2015). The efficacy of LDM therapy has been thought to be mainly caused by its antiangiogenic effects (Kerbel and Kamen, 2004), such as direct cytotoxicity to endothelial cells (Bocci et al., 2002), reduced recruitment of endothelial progenitors (Bertolini et al., 2003), and increased expression of the antiangiogenic factor thrombospondin-1 (Bocci et al., 2003). Recent studies suggest that LDM therapy may also mediate its antitumor effect by inhibiting regulatory T cells (Lutsiak et al., 2005; Ghiringhelli et al., 2007), by triggering the maturation of tumor-infiltrating dendritic cells (Tanaka et al., 2009), or by disrupting cancer stem cell–promoting vascular niches (Folkins et al., 2007). Nonetheless, our study identified a new and important mechanism underlying the enhanced therapeutic efficacy of LDM therapy in CAF-abundant, desmoplastic cancers, which is mediated through an attenuated STAT-1 and NF-κB activation in CAFs leading to a substantially reduced ELR^+ chemokine production, thereby significantly tempering the therapy-triggered stromal pro-oncogenic activity. Of note, previous studies have indi-

CD298, CD44, and CD24 staining of carcinoma cells with the frequency of the boxed $CD44^+CD24^{-/low}$ cell population as a percentage of $CD298^+$ cancer cells shown. (Right) The percentages of $CD298^+CD44^+CD24^{-/low}$ cells relative to the $CD298^+$ carcinoma cells isolated from the tumors. Data from three independent experiments ($n = 3$ in each group) are shown. FSC, forward scatter. Data are mean ± SEM; Student's *t* test. *, $P < 0.05$ vs. vehicle. †, $P < 0.05$ vs. MTD.

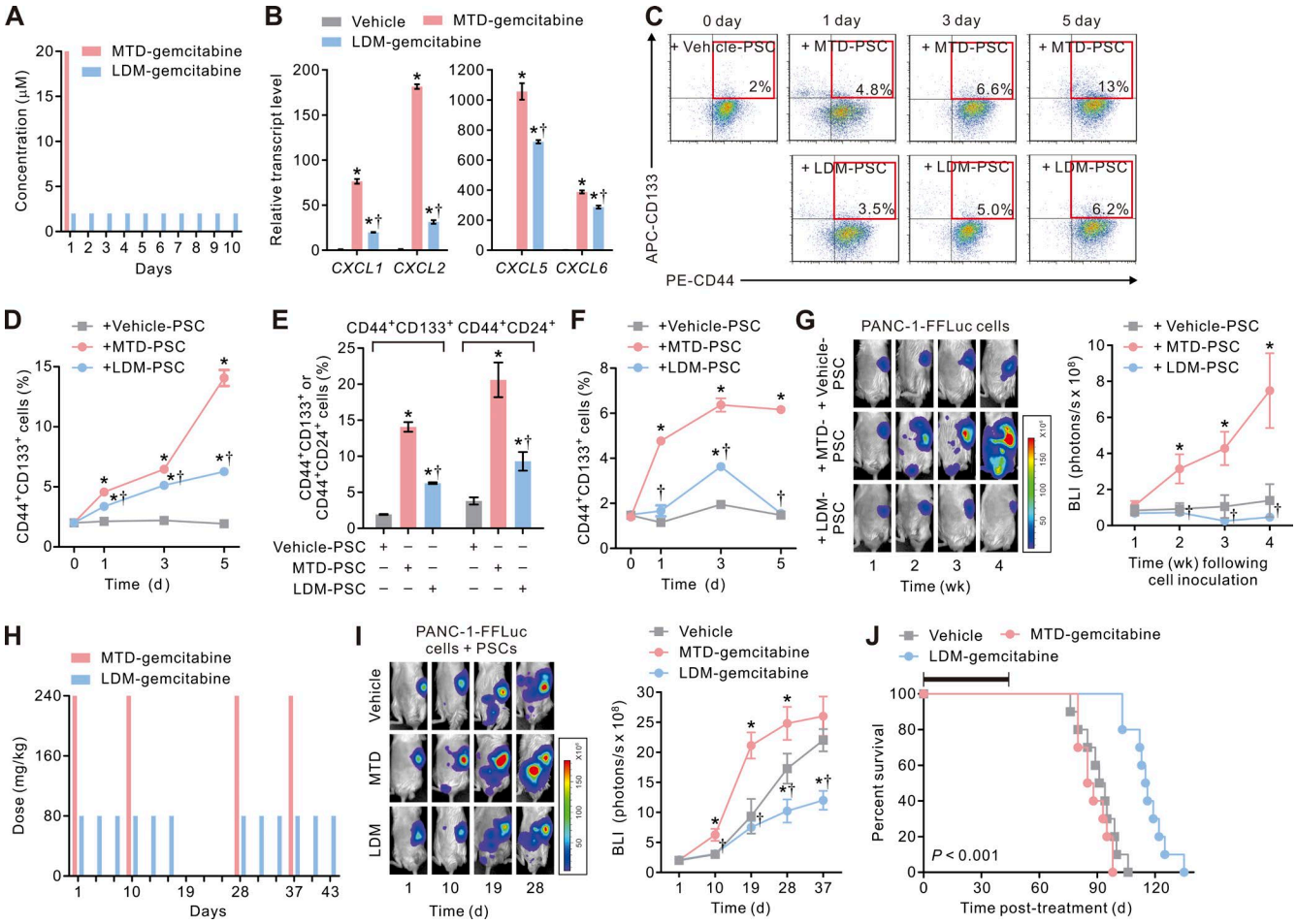

Figure 9. **LDM chemotherapy enhances treatment response in desmoplastic PDAC.** (A) Schematic showing in vitro gemcitabine treatment protocols that mimic MTD (20 μM × 30 min on the first day, followed by a drug-free interval of 9 d) and LDM (2 μM × 30 min daily for 10 consecutive days) chemotherapy regimens. (B) The transcript levels of the ELR$^+$ chemokines in vehicle (vehicle-PSC)-, MTD (MTD-PSC)-, or LDM-gemcitabine (LDM-PSC)–treated PSCs. Data from three independent experiments (n = 3 in each group; *, $P < 0.05$ vs. vehicle-gemcitabine; †, $P < 0.05$ vs. MTD-gemcitabine) are shown. (C) Vehicle-, MTD-, or LDM-PSCs were co-cultivated with PANC-1 carcinoma cells in a dual-chamber apparatus for 5 d, and the carcinoma cells were subjected to flow cytometric analyses. Shown are representative plots showing patterns of CD44 and CD133 staining of cells at different times in the co-culture, with the frequency of the boxed CD44$^+$CD133$^+$ cell population as a percentage of cancer cells shown. (D) The percentages of CD44$^+$CD133$^+$ carcinoma cells at different times in the co-culture in C. Data from three independent experiments (n = 3 in each group; *, $P < 0.05$ vs. vehicle-PSC; †, $P < 0.05$ vs. MTD-PSC) are shown. (E) The percentages of CD44$^+$CD133$^+$ or CD44$^+$CD24$^+$ carcinoma cells at day 5 in the co-culture. Data from three independent experiments (n = 3 in each group; *, $P < 0.05$ vs. vehicle-PSC; †, $P < 0.05$ vs. MTD-PSC) are shown. (F) Vehicle-, MTD-, or LDM-PSCs were co-cultivated with primary SP-1 PDAC cells , and the percentages of CD44$^+$CD133$^+$ TICs were analyzed. Data from three independent experiments (n = 3 in each group; *, $P < 0.05$ vs. vehicle-PSC; †, $P < 0.05$ vs. MTD-PSC) are shown. (G) Vehicle-, MTD-, or LDM-PSCs were co-injected with FFLuc-transduced PANC-1 carcinoma cells into the pancreatic tails of NOG mice. Tumor bulk was then monitored using BLI. (Left) Shown is representative BLI of tumors at the indicated time after cell inoculation. (Right) Tumor bulk quantified as BLI normalized photon counts as a function of time. Data from one experiment (n = 6 in each group; *, $P < 0.05$ vs. vehicle-PSC; †, $P < 0.05$ vs. MTD-PSC) are shown. (H) PSCs were co-injected with PANC-1 cells into the pancreatic tails of HSC-hu-NOG mice. 10 d later, the tumor-bearing mice received intraperitoneal injections of vehicle or gemcitabine using an MTD (240 mg/kg every 9 d for 18 d followed by a 9-d rest and then another 18-d treatment cycle)- or an LDM (80 mg/kg every 3 d for 18 d followed by a 9-d rest and then another 18-d treatment cycle)-mimetic regimen. (I, left) Representative BLI of tumors at the indicated time after initiation of the therapy as described in H. (Right) Tumor bulk quantified as BLI normalized photon counts as a function of time. Data from one experiment (n = 3 in each group; *, $P < 0.05$ vs. vehicle-gemcitabine; †, $P < 0.05$ vs. MTD-gemcitabine) are shown. (B, D–G, and I) Data are mean ± SEM; Student's t test. (J) Percent survival as a function of time in mice described in I. The black bar indicates the duration of treatment. Data from one experiment (n = 3 in each group; the survival curves were compared using log-rank test; LDM vs. MTD) are shown.

cated that the antiangiogenic and antitumor effects of LDM chemotherapy are specifically observed in certain chemotherapeutic agents, which does not include doxorubicin (Bocci et al., 2002). Nonetheless, in our CAF-abundant tumor model, which resembles human desmoplastic breast cancer, doxorubicin treatments administered using an LDM-mimetic reg-

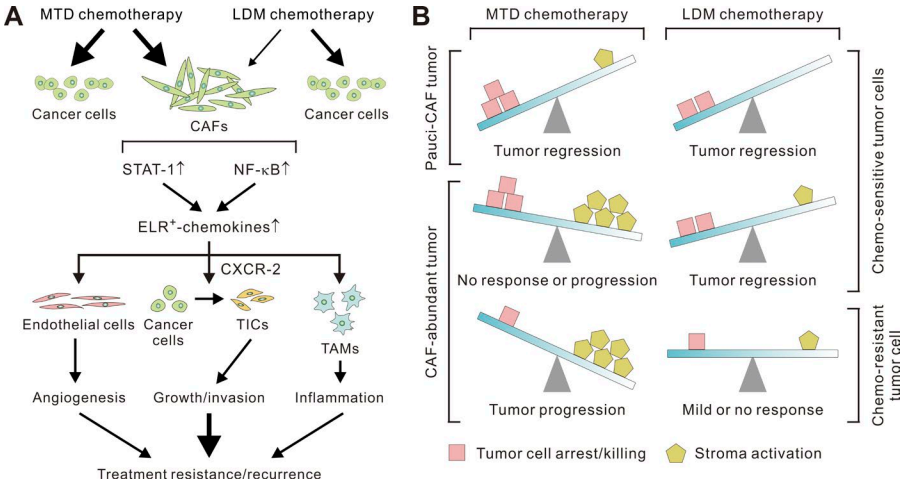

Figure 10. **The beneficial effects of LDM chemotherapy in desmoplastic cancers.** (A) Schematic showing the proposed mechanisms underlying the pro-oncogenic functions of MTD-CAFs that serve to antagonize the antitumor efficacy and lead to tumor recurrence and/or metastasis, whereas chemotherapy at LDM therapy regimens can exempt the stroma from these treatment-elicited stromal-epithelial signaling events. (B) Both MTD and LDM chemotherapy can lead to regression of tumors with few CAFs in their stroma (i.e., pauci-CAF tumor), whereas in CAF-abundant (i.e., desmoplastic) tumors, MTD chemotherapy induces strong and persistent stroma activation, which undermines the treatment response. MTD chemotherapy may paradoxically promote tumor progression in certain contexts depending on the treatment sensitivity of carcinoma cells and the relative abundance of CAFs or other types of stroma cells. LDM chemotherapy can avoid the inadvertent activation of the tumor stroma, whereby it can enhance the treatment response.

imen could greatly enhance the treatment response of the tumors. Thus, our results not only highlight the importance of CAF and stroma response in cancer therapy, but also may further broaden the clinical applicability of LDM therapy.

Recent evidence suggests that TICs exist in a dynamic equilibrium with their microenvironments, and the TIC phenotype is tightly regulated by cell-extrinsic factors derived by their surrounding cells or the stroma. In keeping with this paradigm, inflammatory mediators, such as IL-6 and IL-8, have been found to be critically involved in the regulation of TICs and their contribution to cancer invasion and metastasis (Iliopoulos et al., 2011; Korkaya et al., 2011, 2012). Nevertheless, these observations were made in untreated and chemo-naive tumors, whereas our results suggest that, in chemo-treated tumors, ELR^+ chemokines play a major role in the regulation of TICs especially those with mesenchymal-like properties. In this regard, the substantial amounts of these pro-TIC ELR^+ chemokines produced by MTD-treated CAFs within the treated tumors may contribute significantly to the significant enrichment of TICs in breast cancers after neoadjuvant chemotherapy (Li et al., 2008; Creighton et al., 2009). Our study additionally suggests that this CAF ELR^+ chemokine phenotype is potently induced by MTD chemotherapy but can be largely avoided by switching to LDM therapy regimens. Our study thus may not only trigger more clinical trials dedicated to comparing the effects of MTD and LDM chemotherapy on the tumor stroma and TICs and examining their efficacy in human desmoplastic cancers, but also may help the identification of the cancer patients who will most likely benefit from LDM chemotherapy to guide the design of tumor-tailored and personalized chemotherapy regimens.

In summary, our findings suggest that systemic chemotherapy has a significant impact on the stroma that is associated with human desmoplastic cancers that includes sustained activation of CAFs leading to pro-oncogenic and pro-TIC paracrine signaling activities. We delineated the signaling pathway that mediates this characteristic stromal response to chemotherapy and identified an effective way to attenuate it by using LDM therapy regimens. Our results lend support to the emerging paradigm that maintains that stroma-derived signals contribute to tumor pathology and suggests that LDM therapy or targeting the paracrine signaling mediated by chemo-treated CAFs may be a valid approach for improving therapeutic outcome in desmoplastic cancers.

MATERIALS AND METHODS

Human cancer specimens, staining, and cell isolation

Tumor specimens were excised from a cohort of 15 breast cancer patients who had not received prior chemotherapy in the Tung's Metro-harbor Hospital, Taiwan (the TMH cohort; Table S1). The specimens were processed within 3 h of tumor removal by mechanical dissociation, enzymatic digestion, and differential centrifugation, as described previously (Tsuyada et al., 2012), followed by sequential magnetic-assisted cell sorting using antifibroblast MicroBeads and a magnetic-assisted cell-sorting Dead Cell Removal kit (Miltenyi Biotec). Fibroblasts were plated on collagen-coated tissue culture plates and maintained in DMEM (Invitrogen) supplemented with 15% FBS. Carcinoma cells were cultured in IMDM (Invitrogen) supplemented with glutamine, insulin, transferrin, selenium (all from Lonza), and 20% FBS (Tsuyada et al., 2012). Using this protocol, we were able to isolate three pairs of cognate carcinoma cells and CAFs that could be propagated for >15

passages to permit subsequent experiments. Carcinoma cells were confirmed to be aneuploid according to karyotyping. All human tissues were collected using protocols approved by the Institutional Review Boards at Tung'Taichung Metroharbor Hospital. Primary PDAC SP-1 cells were isolated from the malignant ascites of a patient with metastatic PDAC (a gift from Y.-S. Shan, National Cheng Kung University Hospital, Tainan, Taiwan). HCC-1954, MCF-7, HCC-1806, HCC-38, BT-474, MDA-MB-436, PANC-1, and U-937 cells (all from ATCC) and PSCs (a gift from M. Löhr, German Cancer Research Center, Heidelberg, Germany; Jesnowski et al., 2005) were cultured and propagated according to the providers' recommendations.

Treatment of CAFs and PSCs

Minimally passaged (less than three passages) primary breast CAFs were treated with doxorubicin, paclitaxel, or 4H-CPA (all from Sigma-Aldrich) according to the MTD- or the LDM-mimetic scheme described in Fig. 1 B or Fig. 5 (A, C, and E) (Struck et al., 1987; Twelves et al., 1991; Fogli et al., 2002). PSCs were maintained in DMEM supplemented with 10% FBS and treated with gemcitabine (LIL LY France) according to the dose schemes described in Fig. 9 A. After the completion of treatments, fibroblasts were washed twice with Dulbecco's PBS, replenished with drug-free culture media, and then allowed to recover for 14 d after initiation of the treatment. Dead cells that had detached from the culture surface were removed and excluded from subsequent experiments.

Immunoblot analysis

Immunoblot protein analysis was performed according to standard protocols. Antibodies used included anti–human α-SMA (1A4; Dako), p16 (DCS-50; Abcam), STAT-1 (1/Stat1; BD), phospho–STAT-1 (Tyr701), NF-κB p65 (C22B4), phospho-IκBα (Ser32/36; 5A5; Cell Signaling Technology), anti-IκBα (6A920), and histone 2B (FL-126; Santa Cruz Biotechnology, Inc.).

Gene expression profiling and clustering analysis

Total RNA samples were extracted using TRIzol (Invitrogen) and then purified using an RNeasy mini-kit (QIAGEN). Gene expression analysis was performed on a GeneChip platform (Human Genome U133A 2.0 Plus; Affymetrix) according to the manufacturer's instructions. The gene expression data were deposited in NCBI's Gene Expression Omnibus (GEO) and are accessible under accession no. GSE23399. Differentially expressed genes were selected using Student's *t* test or Tukey's honestly significant difference test ($P < 0.05$; fold-change > 2×). The genes were functionally annotated using DAVID, and the enriched functional gene categories identified were further processed and displayed using Cytoscape. Hierarchical clustering of the selected genes was performed using Cluster and TreeView software.

Quantitative real-time PCR (qRT-PCR) and ELISA analyses

qRT-PCR analysis was performed on the amplified RNA using the LightCycler FastStart DNA Masterplus SYBR Green I kit (Roche) according to the manufacturer's instructions. Oligonucleotide primers were designed using LightCycler Probe Design software (Roche) or Primer Bank. Transcript expression was quantified by normalizing the gene of interest copy number (per microliter) to absolute levels of an endogenous, stably expressed reference gene, ribosomal protein L13a (RPL13A). ELISA was performed using kits according to the manufacturer's instructions (R&D Systems).

3D co-culture assay

Breast carcinoma cells were co-cultivated with CAFs on top of a multicomponent 3D extracellular matrix hydrogel consisting of growth factor–reduced reconstituted basement membrane (Matrigel) and type I collagen (both from BD) at a 1:1 ratio (Tsai et al., 2005).

Cell death assay

Cell death was analyzed by a two-color fluorescence cell viability assay by counting the nuclei of dead cells using CYTOX-orange dye (Invitrogen) and normalizing dead cells to total cell number estimated by counterstaining nuclei with Hoechst 33342 (Invitrogen). In selected experiments (Fig. 1 C), cells were stained with active caspase-3 (E83-77; Abcam) for the detection of apoptosis.

In vivo tumor models and analyses

In the orthotopic mouse models of desmoplastic breast cancer, NHRI-BC-011, HCC-1954, or MDA-MB-436 cells were lentivirally transduced by a GFP and FFLuc fusion vector (UBC-EGFP-T2A-Luc; System Biosciences), and GFP-positive cells were enriched by FACS. In the orthotopic breast cancer model, 5×10^5 cells carcinoma cells and 10^6 CAFs in 100 µl (1:1 Matrigel/cells) were inoculated into the mammary fat pads of female NOG mice or HSC-hu-NOG mice (National Institute of Infectious Diseases and Vaccinology, Taiwan). Successful engraftment of HSCs was validated by determining the titers of human IgM and IgG and accessing human $CD45^+$, $CD3^+$, and $CD19^+$ cells in the peripheral blood at 8–12 wk after HSC engrafting. In selected experiments (Figs. 4 D and 7 D), the cells were inoculated subcutaneously into the flanks of 8-wk-old female nude mice (National Laboratory Animal Center, National Applied Research Laboratories, Taiwan). In the orthotopic mouse model of desmoplastic PDAC, 5×10^5 FFLuc-transduced PANC-1 PDAC cells (ATCC) and 10^6 PSCs were inoculated into the pancreatic tail of NOG mice or HSC-hu-NOG mice. In selective experiments, the mice were given 0.5 mg/kg/day CXCR-2 inhibitor SB225002 by intraperitoneal injections 2 d before and after chemotherapy treatments. Tumor mass was quantified weekly by bioluminescence (IVIS Imaging System; Caliper Life Sciences) according to the manufacturer's directions. Protocols for animal care and experimentation were ap-

proved by the Institutional Animal Care and Use Committee of the National Health Research Institutes, Taiwan, and were adhered to the National Institutes of Health Guide for the Care and Use of Laboratory Animals.

In the PDX breast tumor model, NOD-SCID γ (NSG) mice bearing PDX breast tumors (TM00999) derived from a triple-negative ($ER^-PR^-HER2^-$) breast tumor were purchased from The Jackson Laboratory. When tumors became palpable, the mice were administered with MTD- or LDM-doxorubicin or vehicle intraperitoneally according to the protocol described in Fig. 7 C, and the tumors were calipered weekly to monitor growth kinetics. Tumor volumes were calculated using the formula 0.5 × length × $(\text{width})^2$. The animals were euthanized 31 d after initiation of the treatments.

LCM

LCM of breast tumor tissues obtained from the TMH cohort (Table S1) was performed as previously described (Finak et al., 2008) with modifications. In brief, three 7-µm sections each were serially cut from snap-frozen tumor tissues, placed onto a polyethylene naphthalate membrane slide, and stained with a HistoGene LCM Staining kit to isolate distinct CAF- or cancer cell–enriched regions, as identified by an expert pathologist (W.-Y. Chen), by using the Veritas automated LCM system (Arcturus Engineering). Approximately 1,500 cells were collected onto the Capsure Macro cap, and the RNA sample was extracted using a Picopure RNA Isolation kit. qRT-PCR assay was performed as described.

Transwell invasion assay

Cancer cell– or PMA (5 nM × 72 h)-primed U937 cells (for in vitro macrophage differentiation) were seeded on Transwell inserts (BD) with a thin layer of growth factor–reduced Matrigel (BD) coating with CAFs seeded in the lower compartments of the Transwell. After an incubation period of 12 h, the cells that invaded through the insert membrane were fixed, stained with CYTOX-green (Invitrogen), and counted using a fluorescence microscope.

Immunofluorescent staining and confocal imaging

Immunofluorescent staining of cells grown on culture plastics was performed using standard protocols. Whole-culture immunofluorescence staining of cells grown in 3D co-culture was executed as previously described (Lee et al., 2007). Confocal imaging was performed using a confocal microscope system (Digital Eclipse C1; Nikon).

Immunohistochemical staining

Formalin-fixed, paraffin-embedded human or mouse tumor tissues were processed using standard protocols, stained with anti–α-SMA (for detection of CAFs; α sm-1; Abcam), anti-F4/80 (for detection of TAMs; Hycult Biotech), anti–Fizz-1 (for detection of M2-subtype TAMs; Abcam), or anti–p–STAT-1 (for detection in CAFs; Cell Signaling Technology) and then detected by using a Dako EnVision kit. All staining was evaluated by an expert pathologist (W.-Y. Chen).

Reporter assay

Lentivirus-mediated expression of the STAT-1 or NF-κB luciferase reporter vector as well as the reporter assay were performed according to the provider's recommendations (Cignal Lenti Reporter; SABiosciences).

Manipulation of gene expression

Functional inhibition of STAT-1 or NF-κB activity in CAFs was achieved by generating lentiviral expression constructs for a phosphorylation-deficient mutant of STAT-1–super-repressor (STAT-1–SR; STAT-1–SRpLVX-puro–STAT-1–SR), or a phosphorylation-resistant mutant of IκBα (pLVX-puro-IκB α-SR mutant; NFKBIA-SR; Kuperwasser et al., 2004) and infecting them in minimally passaged NHRI-BCAF-011 CAFs. pLVX-puro–STAT-1–SR was generated by subcloning eGFP–STAT-1–Y701F (Addgene) into the pLVX-IRES-puro (Takara Bio Inc.), which was followed by a serine for leucine substation at amino acid 706 (L706S) to impair the phosphorylation, homodimerization, and nuclear translocation of STAT-1 (Dupuis et al., 2001). Lentivirus production and cell infection were performed according to the manufacturer's protocols (Takara Bio Inc.). The human B cell CLL/lymphoma 2 (Bcl-2) expression construct pBABE-puro-Bcl2 was obtained from Addgene. Amphotropic retrovirus was produced in Phoenix ampho cells (gift from G. Nolan, Stanford University, Stanford, CA) using the packaging vectors pCgp and pVSV-G to boost viral titer.

Flow cytometry and tumorsphere assays

Cancer cells were dissociated, antibody labeled (1–2 µg per 10^6 cells × 1 h), and resuspended in HBSS/2% FBS as previously described (Al-Hajj et al., 2003; Li et al., 2007). The antibodies used include APC–anti-CD44, PE–anti-CD44, FITC–anti-CD24, Alexa Fluor 647–anti-CD24 (all from BD), APC–anti-CD133 (Miltenyi Biotec), and anti-CD298 (LNH-94; BioLegend). Flow cytometry was done using a FACSCanto II flow cytometer (BD) with the electronic gating set according to cells stained with the corresponding isotype-matched control IgG. In selected experiments, cancer cells were cultured in the presence of 1 µM SB225002 (EMD Millipore) or a neutralizing antibody directed against 10 µg/ml CXCL-1 (clone 20326; R&D Systems), 10 µg/ml CXCL-2 (Abcam), 10 µg/ml CXCL-5 (R&D Systems), or 10 µg/ml CXCL-6 (clone 60910; R&D Systems) before the flow cytometry analysis. The ALDEFLUOR assay (STEMCELL Technologies) was performed according to the manufacturer's recommendation.

To assess the tumorsphere formation efficiency of TICs, $CD44^+CD24^{low/-}$ cells and $CD133^+CD44^+$ cells were FACS sorted from breast cancer cells and PDAC cells, respectively, using a FACSAria III cell sorter (BD). The tumorsphere assay for breast TICs was performed using the MammoCult Human

Medium kit (STEMCELL Technologies). The tumorsphere assay for pancreatic TICs was performed as previously described (Arensman et al., 2014). For limiting dilution assay, $CD44^+CD24^{low/-}$ cells were plated in limiting dilution (200, 100, and 50 cells per well) in 96-well plates in the respective culture media. The presence of spheres was evaluated after 5 d.

Statistical analysis

The statistical programming language R and SPSS 10.0 software were used to conduct the statistical analysis of our data. A two-tailed Student's *t* test was used for simple significance testing. Survival curves were generated using the Kaplan-Meier method. The curves were plotted and compared using the log-rank test using Prism 5.02 (GraphPad Software). The data from the limiting dilution assay were analyzed and plotted using ELDA software. The likelihood ratio test and χ^2 test were used to assess the significance.

Online supplemental material

Fig. S1 shows the gating strategy and flow cytometric analysis of $CD44^+CD24^{-/low}$ breast carcinoma cells. Fig. S2 shows the strategy and flow cytometric analysis of $CD44^+CD24^{-/low}$ carcinoma cells in PDX breast tumors. Fig. S3 shows the gating strategy and flow cytometric analysis of $CD133^+CD44^+$ PDAC cells. Fig. S4 shows the patterns of CD44 and CD133 staining of primary SP-1 cells in the cancer cell/PSC co-culture. Table S1 shows clinical characteristics of the breast tumors used for cell isolation and LCM experiments.

ACKNOWLEDGMENTS

This work was supported in part by grants from the Ministry of Science and Technology, Taiwan (MOST 102-2628-B-400-MY3, MOST 103-2314-B-400-019, MOST 104-2314-B-400-022-MY3, and MOST 105-2314-B-400-018-MY3 to K.K. Tsai), grants from the National Health Research Institutes, Taiwan (NHRI CA-103-SP-01 and NHRI-014-A1-CASP01-014 to K.K. Tsai), grants from the US Department of Defense Breast Cancer Research Program (BC122990 to V.M. Weaver), a grant from Taipei Medical University, Wan Fang Hospital (104-wf-phd-01 to T.S. Chan), and grants from the National Cancer Institute at the National Institutes of Health, USA (R01 CA174929 and CA192914-01 to V.M. Weaver). S.S. Huang conducted his thesis research under the auspices of the Graduate Program of Biotechnology in Medicine, National Tsing Hua University, and the National Health Research Institutes.

The authors declare no competing financial interests.

Submitted: 22 October 2015
Revised: 8 June 2016
Accepted: 21 October 2016

REFERENCES

Al-Hajj, M., M.S. Wicha, A. Benito-Hernandez, S.J. Morrison, and M.F. Clarke. 2003. Prospective identification of tumorigenic breast cancer cells. *Proc. Natl. Acad. Sci. USA.* 100:3983–3988. http://dx.doi.org/10.1073/pnas.0530291100

Ali, S., and G. Lazennec. 2007. Chemokines: novel targets for breast cancer metastasis. *Cancer Metastasis Rev.* 26:401–420. http://dx.doi.org/10.1007/s10555-007-9073-z

Arensman, M.D., A.N. Kovochich, R.M. Kulikauskas, A.R. Lay, P.T. Yang, X. Li, T. Donahue, M.B. Major, R.T. Moon, A.J. Chien, and D.W. Dawson. 2014. WNT7B mediates autocrine Wnt/β-catenin signaling and anchorage-independent growth in pancreatic adenocarcinoma. *Oncogene.* 33:899–908. http://dx.doi.org/10.1038/onc.2013.23

Beck, B., G. Driessens, S. Goossens, K.K. Youssef, A. Kuchnio, A. Caauwe, P.A. Sotiropoulou, S. Loges, G. Lapouge, A. Candi, et al. 2011. A vascular niche and a VEGF-Nrp1 loop regulate the initiation and stemness of skin tumours. *Nature.* 478:399–403. http://dx.doi.org/10.1038/nature10525

Bertolini, F., S. Paul, P. Mancuso, S. Monestiroli, A. Gobbi, Y. Shaked, and R.S. Kerbel. 2003. Maximum tolerable dose and low-dose metronomic chemotherapy have opposite effects on the mobilization and viability of circulating endothelial progenitor cells. *Cancer Res.* 63:4342–4346.

Bocci, G., K.C. Nicolaou, and R.S. Kerbel. 2002. Protracted low-dose effects on human endothelial cell proliferation and survival in vitro reveal a selective antiangiogenic window for various chemotherapeutic drugs. *Cancer Res.* 62:6938–6943.

Bocci, G., G. Francia, S. Man, J. Lawler, and R.S. Kerbel. 2003. Thrombospondin 1, a mediator of the antiangiogenic effects of low-dose metronomic chemotherapy. *Proc. Natl. Acad. Sci. USA.* 100:12917–12922. http://dx.doi.org/10.1073/pnas.2135406100

Bruchard, M., G. Mignot, V. Derangère, F. Chalmin, A. Chevriaux, F. Végran, W. Boireau, B. Simon, B. Ryffel, J.L. Connat, et al. 2013. Chemotherapy-triggered cathepsin B release in myeloid-derived suppressor cells activates the Nlrp3 inflammasome and promotes tumor growth. *Nat. Med.* 19:57–64. http://dx.doi.org/10.1038/nm.2999

Calabrese, C., H. Poppleton, M. Kocak, T.L. Hogg, C. Fuller, B. Hamner, E.Y. Oh, M.W. Gaber, D. Finklestein, M. Allen, et al. 2007. A perivascular niche for brain tumor stem cells. *Cancer Cell.* 11:69–82. http://dx.doi.org/10.1016/j.ccr.2006.11.020

Chen, W.J., C.C. Ho, Y.L. Chang, H.Y. Chen, C.A. Lin, T.Y. Ling, S.L. Yu, S.S. Yuan, Y.J. Chen, C.Y. Lin, et al. 2014. Cancer-associated fibroblasts regulate the plasticity of lung cancer stemness via paracrine signalling. *Nat. Commun.* 5:3472.

Cheng, J.D., R.L. Dunbrack Jr., M. Valianou, A. Rogatko, R.K. Alpaugh, and L.M. Weiner. 2002. Promotion of tumor growth by murine fibroblast activation protein, a serine protease, in an animal model. *Cancer Res.* 62:4767–4772.

Creighton, C.J., X. Li, M. Landis, J.M. Dixon, V.M. Neumeister, A. Sjolund, D.L. Rimm, H. Wong, A. Rodriguez, J.I. Herschkowitz, et al. 2009. Residual breast cancers after conventional therapy display mesenchymal as well as tumor-initiating features. *Proc. Natl. Acad. Sci. USA.* 106:13820–13825. http://dx.doi.org/10.1073/pnas.0905718106

Daenen, L.G., J.M. Roodhart, M. van Amersfoort, M. Dehnad, W. Roessingh, L.H. Ulfman, P.W. Derksen, and E.E. Voest. 2011. Chemotherapy enhances metastasis formation via VEGFR-1–expressing endothelial cells. *Cancer Res.* 71:6976–6985. http://dx.doi.org/10.1158/0008-5472.CAN-11-0627

Dupuis, S., C. Dargemont, C. Fieschi, N. Thomassin, S. Rosenzweig, J. Harris, S.M. Holland, R.D. Schreiber, and J.L. Casanova. 2001. Impairment of mycobacterial but not viral immunity by a germline human STAT1 mutation. *Science.* 293:300–303. http://dx.doi.org/10.1126/science.1061154

Erez, N., M. Truitt, P. Olson, S.T. Arron, and D. Hanahan. 2010. Cancer-associated fibroblasts are activated in incipient neoplasia to orchestrate tumor-promoting inflammation in an NF-κB-dependent manner. *Cancer Cell.* 17:135–147. http://dx.doi.org/10.1016/j.ccr.2009.12.041

Finak, G., N. Bertos, F. Pepin, S. Sadekova, M. Souleimanova, H. Zhao, H. Chen, G. Omeroglu, S. Meterissian, A. Omeroglu, et al. 2008. Stromal gene expression predicts clinical outcome in breast cancer. *Nat. Med.* 14:518–527. http://dx.doi.org/10.1038/nm1764

Fogli, S., R. Danesi, A. Gennari, S. Donati, P.F. Conte, and M. Del Tacca. 2002. Gemcitabine, epirubicin and paclitaxel: pharmacokinetic and

pharmacodynamic interactions in advanced breast cancer. *Ann. Oncol.* 13:919–927. http://dx.doi.org/10.1093/annonc/mdf164

Folkins, C., S. Man, P. Xu, Y. Shaked, D.J. Hicklin, and R.S. Kerbel. 2007. Anticancer therapies combining antiangiogenic and tumor cell cytotoxic effects reduce the tumor stem-like cell fraction in glioma xenograft tumors. *Cancer Res.* 67:3560–3564. http://dx.doi.org/10.1158/0008-5472.CAN-06-4238

Ghiringhelli, F., C. Menard, P.E. Puig, S. Ladoire, S. Roux, F. Martin, E. Solary, A. Le Cesne, L. Zitvogel, and B. Chauffert. 2007. Metronomic cyclophosphamide regimen selectively depletes $CD4^+CD25^+$ regulatory T cells and restores T and NK effector functions in end stage cancer patients. *Cancer Immunol. Immunother.* 56:641–648. http://dx.doi.org/10.1007/s00262-006-0225-8

Ginestier, C., M.H. Hur, E. Charafe-Jauffret, F. Monville, J. Dutcher, M. Brown, J. Jacquemier, P. Viens, C.G. Kleer, S. Liu, et al. 2007. ALDH1 is a marker of normal and malignant human mammary stem cells and a predictor of poor clinical outcome. *Cell Stem Cell.* 1:555–567. http://dx.doi.org/10.1016/j.stem.2007.08.014

Gingis-Velitski, S., D. Loven, L. Benayoun, M. Munster, R. Bril, T. Voloshin, D. Alishekevitz, F. Bertolini, and Y. Shaked. 2011. Host response to short-term, single-agent chemotherapy induces matrix metalloproteinase-9 expression and accelerates metastasis in mice. *Cancer Res.* 71:6986–6996. http://dx.doi.org/10.1158/0008-5472.CAN-11-0629

Goetz, J.G., S. Minguet, I. Navarro-Lérida, J.J. Lazcano, R. Samaniego, E. Calvo, M. Tello, T. Osteso-Ibáñez, T. Pellinen, A. Echarri, et al. 2011. Biomechanical remodeling of the microenvironment by stromal caveolin-1 favors tumor invasion and metastasis. *Cell.* 146:148–163. http://dx.doi.org/10.1016/j.cell.2011.05.040

Grunewald, R., H. Kantarjian, M. Du, K. Faucher, P. Tarassoff, and W. Plunkett. 1992. Gemcitabine in leukemia: a phase I clinical, plasma, and cellular pharmacology study. *J. Clin. Oncol.* 10:406–413.

Hasnis, E., D. Alishekevitz, S. Gingis-Veltski, R. Bril, E. Fremder, T. Voloshin, Z. Raviv, A. Karban, and Y. Shaked. 2014. Anti-Bv8 antibody and metronomic gemcitabine improve pancreatic adenocarcinoma treatment outcome following weekly gemcitabine therapy. *Neoplasia.* 16:501–510. http://dx.doi.org/10.1016/j.neo.2014.05.011

Hidalgo, M., F. Amant, A.V. Biankin, E. Budinská, A.T. Byrne, C. Caldas, R.B. Clarke, S. de Jong, J. Jonkers, G.M. Mælandsmo, et al. 2014. Patient-derived xenograft models: an emerging platform for translational cancer research. *Cancer Discov.* 4:998–1013. http://dx.doi.org/10.1158/2159-8290.CD-14-0001

Hughes, R., B.Z. Qian, C. Rowan, M. Muthana, I. Keklikoglou, O.C. Olson, S. Tazzyman, S. Danson, C. Addison, M. Clemons, et al. 2015. Perivascular M2 macrophages stimulate tumor relapse after chemotherapy. *Cancer Res.* 75:3479–3491. http://dx.doi.org/10.1158/0008-5472.CAN-14-3587

Iliopoulos, D., H.A. Hirsch, G. Wang, and K. Struhl. 2011. Inducible formation of breast cancer stem cells and their dynamic equilibrium with non-stem cancer cells via IL6 secretion. *Proc. Natl. Acad. Sci. USA.* 108:1397–1402. http://dx.doi.org/10.1073/pnas.1018898108

Jesnowski, R., D. Fürst, J. Ringel, Y. Chen, A. Schrödel, J. Kleeff, A. Kolb, W.D. Schareck, and M. Löhr. 2005. Immortalization of pancreatic stellate cells as an in vitro model of pancreatic fibrosis: deactivation is induced by matrigel and *N*-acetylcysteine. *Lab. Invest.* 85:1276–1291. http://dx.doi.org/10.1038/labinvest.3700329

Jung, J.H., S.J. Lee, J. Kim, S. Lee, H.J. Sung, J. An, Y. Park, and B.S. Kim. 2015. CXCR2 and its related ligands play a novel role in supporting the pluripotency and proliferation of human pluripotent stem cells. *Stem Cells Dev.* 24:948–961. http://dx.doi.org/10.1089/scd.2014.0381

Kalluri, R., and M. Zeisberg. 2006. Fibroblasts in cancer. *Nat. Rev. Cancer.* 6:392–401. http://dx.doi.org/10.1038/nrc1877

Karnoub, A.E., A.B. Dash, A.P. Vo, A. Sullivan, M.W. Brooks, G.W. Bell, A.L. Richardson, K. Polyak, R. Tubo, and R.A. Weinberg. 2007. Mesenchymal stem cells within tumour stroma promote breast cancer metastasis. *Nature.* 449:557–563. http://dx.doi.org/10.1038/nature06188

Kerbel, R.S., and A. Grothey. 2015. Gastrointestinal cancer: Rationale for metronomic chemotherapy in phase III trials. *Nat. Rev. Clin. Oncol.* 12:313–314. http://dx.doi.org/10.1038/nrclinonc.2015.89

Kerbel, R.S., and B.A. Kamen. 2004. The anti-angiogenic basis of metronomic chemotherapy. *Nat. Rev. Cancer.* 4:423–436. http://dx.doi.org/10.1038/nrc1369

Korkaya, H., S. Liu, and M.S. Wicha. 2011. Breast cancer stem cells, cytokine networks, and the tumor microenvironment. *J. Clin. Invest.* 121:3804–3809. http://dx.doi.org/10.1172/JCI57099

Korkaya, H., G.I. Kim, A. Davis, F. Malik, N.L. Henry, S. Ithimakin, A.A. Quraishi, N. Tawakkol, R. D'Angelo, A.K. Paulson, et al. 2012. Activation of an IL6 inflammatory loop mediates trastuzumab resistance in HER2+ breast cancer by expanding the cancer stem cell population. *Mol. Cell.* 47:570–584. http://dx.doi.org/10.1016/j.molcel.2012.06.014

Kuperwasser, C., T. Chavarria, M. Wu, G. Magrane, J.W. Gray, L. Carey, A. Richardson, and R.A. Weinberg. 2004. Reconstruction of functionally normal and malignant human breast tissues in mice. *Proc. Natl. Acad. Sci. USA.* 101:4966–4971. http://dx.doi.org/10.1073/pnas.0401064101

Lawson, D.A., N.R. Bhakta, K. Kessenbrock, K.D. Prummel, Y. Yu, K. Takai, A. Zhou, H. Eyob, S. Balakrishnan, C.Y. Wang, et al. 2015. Single-cell analysis reveals a stem-cell program in human metastatic breast cancer cells. *Nature.* 526:131–135. http://dx.doi.org/10.1038/nature15260

Lee, G.Y., P.A. Kenny, E.H. Lee, and M.J. Bissell. 2007. Three-dimensional culture models of normal and malignant breast epithelial cells. *Nat. Methods.* 4:359–365. http://dx.doi.org/10.1038/nmeth1015

Levental, K.R., H. Yu, L. Kass, J.N. Lakins, M. Egeblad, J.T. Erler, S.F. Fong, K. Csiszar, A. Giaccia, W. Weninger, et al. 2009. Matrix crosslinking forces tumor progression by enhancing integrin signaling. *Cell.* 139:891–906. http://dx.doi.org/10.1016/j.cell.2009.10.027

Li, C., D.G. Heidt, P. Dalerba, C.F. Burant, L. Zhang, V. Adsay, M. Wicha, M.F. Clarke, and D.M. Simeone. 2007. Identification of pancreatic cancer stem cells. *Cancer Res.* 67:1030–1037. http://dx.doi.org/10.1158/0008-5472.CAN-06-2030

Li, X., M.T. Lewis, J. Huang, C. Gutierrez, C.K. Osborne, M.F. Wu, S.G. Hilsenbeck, A. Pavlick, X. Zhang, G.C. Chamness, et al. 2008. Intrinsic resistance of tumorigenic breast cancer cells to chemotherapy. *J. Natl. Cancer Inst.* 100:672–679. http://dx.doi.org/10.1093/jnci/djn123

Liotta, L.A., and E.C. Kohn. 2001. The microenvironment of the tumour-host interface. *Nature.* 411:375–379. http://dx.doi.org/10.1038/35077241

Liu, S., C. Ginestier, S.J. Ou, S.G. Clouthier, S.H. Patel, F. Monville, H. Korkaya, A. Heath, J. Dutcher, C.G. Kleer, et al. 2011. Breast cancer stem cells are regulated by mesenchymal stem cells through cytokine networks. *Cancer Res.* 71:614–624. http://dx.doi.org/10.1158/0008-5472.CAN-10-0538

Liu, S., Y. Cong, D. Wang, Y. Sun, L. Deng, Y. Liu, R. Martin-Trevino, L. Shang, S.P. McDermott, M.D. Landis, et al. 2014. Breast cancer stem cells transition between epithelial and mesenchymal states reflective of their normal counterparts. *Stem Cell Rep.* 2:78–91. http://dx.doi.org/10.1016/j.stemcr.2013.11.009

Lotti, F., A.M. Jarrar, R.K. Pai, M. Hitomi, J. Lathia, A. Mace, G.A. Gantt Jr., K. Sukhdeo, J. DeVecchio, A. Vasanji, et al. 2013. Chemotherapy activates cancer-associated fibroblasts to maintain colorectal cancer-initiating cells by IL-17A. *J. Exp. Med.* 210:2851–2872. http://dx.doi.org/10.1084/jem.20131195

Loven, D., E. Hasnis, F. Bertolini, and Y. Shaked. 2013. Low-dose metronomic chemotherapy: from past experience to new paradigms in the treatment of cancer. *Drug Discov. Today.* 18:193–201. http://dx.doi.org/10.1016/j.drudis.2012.07.015

Lutsiak, M.E., R.T. Semnani, R. De Pascalis, S.V. Kashmiri, J. Schlom, and H. Sabzevari. 2005. Inhibition of $CD4^+25^+$ T regulatory cell

function implicated in enhanced immune response by low-dose cyclophosphamide. *Blood.* 105:2862–2868. http://dx.doi.org/10.1182/blood-2004-06-2410

McAllister, S.S., and R.A. Weinberg. 2014. The tumour-induced systemic environment as a critical regulator of cancer progression and metastasis. *Nat. Cell Biol.* 16:717–727. http://dx.doi.org/10.1038/ncb3015

Nakasone, E.S., H.A. Askautrud, T. Kees, J.H. Park, V. Plaks, A.J. Ewald, M. Fein, M.G. Rasch, Y.X. Tan, J. Qiu, et al. 2012. Imaging tumor-stroma interactions during chemotherapy reveals contributions of the microenvironment to resistance. *Cancer Cell.* 21:488–503. http://dx.doi.org/10.1016/j.ccr.2012.02.017

Orimo, A., P.B. Gupta, D.C. Sgroi, F. Arenzana-Seisdedos, T. Delaunay, R. Naeem, V.J. Carey, A.L. Richardson, and R.A. Weinberg. 2005. Stromal fibroblasts present in invasive human breast carcinomas promote tumor growth and angiogenesis through elevated SDF-1/CXCL12 secretion. *Cell.* 121:335–348. http://dx.doi.org/10.1016/j.cell.2005.02.034

Pasquier, E., M. Kavallaris, and N. André. 2010. Metronomic chemotherapy: new rationale for new directions. *Nat. Rev. Clin. Oncol.* 7:455–465. http://dx.doi.org/10.1038/nrclinonc.2010.82

Rudnick, J.A., L.M. Arendt, I. Klebba, J.W. Hinds, V. Iyer, P.B. Gupta, S.P. Naber, and C. Kuperwasser. 2011. Functional heterogeneity of breast fibroblasts is defined by a prostaglandin secretory phenotype that promotes expansion of cancer-stem like cells. *PLoS One.* 6:e24605. http://dx.doi.org/10.1371/journal.pone.0024605

Seifert, L., G. Werba, S. Tiwari, N.N. Giao Ly, S. Alothman, D. Alqunaibit, A. Avanzi, R. Barilla, D. Daley, S.H. Greco, et al. 2016. The necrosome promotes pancreatic oncogenesis via CXCL1 and Mincle-induced immune suppression. *Nature.* 532:245–249. http://dx.doi.org/10.1038/nature17403

Serebriiskii, I., R. Castelló-Cros, A. Lamb, E.A. Golemis, and E. Cukierman. 2008. Fibroblast-derived 3D matrix differentially regulates the growth and drug-responsiveness of human cancer cells. *Matrix Biol.* 27:573–585. http://dx.doi.org/10.1016/j.matbio.2008.02.008

Shaked, Y., E. Henke, J.M. Roodhart, P. Mancuso, M.H. Langenberg, M. Colleoni, L.G. Daenen, S. Man, P. Xu, U. Emmenegger, et al. 2008. Rapid chemotherapy-induced acute endothelial progenitor cell mobilization: implications for antiangiogenic drugs as chemosensitizing agents. *Cancer Cell.* 14:263–273. http://dx.doi.org/10.1016/j.ccr.2008.08.001

Sherman, M.H., R.T. Yu, D.D. Engle, N. Ding, A.R. Atkins, H. Tiriac, E.A. Collisson, F. Connor, T. Van Dyke, S. Kozlov, et al. 2014. Vitamin D receptor-mediated stromal reprogramming suppresses pancreatitis and enhances pancreatic cancer therapy. *Cell.* 159:80–93. http://dx.doi.org/10.1016/j.cell.2014.08.007

Shiao, S.L., and L.M. Coussens. 2010. The tumor-immune microenvironment and response to radiation therapy. *J. Mammary Gland Biol. Neoplasia.* 15:411–421. http://dx.doi.org/10.1007/s10911-010-9194-9

Shree, T., O.C. Olson, B.T. Elie, J.C. Kester, A.L. Garfall, K. Simpson, K.M. Bell-McGuinn, E.C. Zabor, E. Brogi, and J.A. Joyce. 2011. Macrophages and cathepsin proteases blunt chemotherapeutic response in breast cancer. *Genes Dev.* 25:2465–2479. http://dx.doi.org/10.1101/gad.180331.111

Sonnenberg, M., H. van der Kuip, S. Haubeis, P. Fritz, W. Schroth, G. Friedel, W. Simon, T.E. Mürdter, and W.E. Aulitzky. 2008. Highly variable response to cytotoxic chemotherapy in carcinoma-associated fibroblasts (CAFs) from lung and breast. *BMC Cancer.* 8:364. http://dx.doi.org/10.1186/1471-2407-8-364

Struck, R.F., D.S. Alberts, K. Horne, J.G. Phillips, Y.M. Peng, and D.J. Roe. 1987. Plasma pharmacokinetics of cyclophosphamide and its cytotoxic metabolites after intravenous versus oral administration in a randomized, crossover trial. *Cancer Res.* 47:2723–2726.

Sun, Y., J. Campisi, C. Higano, T.M. Beer, P. Porter, I. Coleman, L. True, and P.S. Nelson. 2012. Treatment-induced damage to the tumor microenvironment promotes prostate cancer therapy resistance through WNT16B. *Nat. Med.* 18:1359–1368. http://dx.doi.org/10.1038/nm.2890

Tanaka, H., H. Matsushima, A. Nishibu, B.E. Clausen, and A. Takashima. 2009. Dual therapeutic efficacy of vinblastine as a unique chemotherapeutic agent capable of inducing dendritic cell maturation. *Cancer Res.* 69:6987–6994. http://dx.doi.org/10.1158/0008-5472.CAN-09-1106

te Poele, R.H., A.L. Okorokov, L. Jardine, J. Cummings, and S.P. Joel. 2002. DNA damage is able to induce senescence in tumor cells in vitro and in vivo. *Cancer Res.* 62:1876–1883.

Tsai, K.K., E.Y. Chuang, J.B. Little, and Z.M. Yuan. 2005. Cellular mechanisms for low-dose ionizing radiation-induced perturbation of the breast tissue microenvironment. *Cancer Res.* 65:6734–6744. http://dx.doi.org/10.1158/0008-5472.CAN-05-0703

Tsuyada, A., A. Chow, J. Wu, G. Somlo, P. Chu, S. Loera, T. Luu, A.X. Li, X. Wu, W. Ye, et al. 2012. CCL2 mediates cross-talk between cancer cells and stromal fibroblasts that regulates breast cancer stem cells. *Cancer Res.* 72:2768–2779. http://dx.doi.org/10.1158/0008-5472.CAN-11-3567

Twelves, C.J., N.A. Dobbs, M. Aldhous, P.G. Harper, R.D. Rubens, and M.A. Richards. 1991. Comparative pharmacokinetics of doxorubicin given by three different schedules with equal dose intensity in patients with breast cancer. *Cancer Chemother. Pharmacol.* 28:302–307.

Vermeulen, L., F. De Sousa E Melo, M. van der Heijden, K. Cameron, J.H. de Jong, T. Borovski, J.B. Tuynman, M. Todaro, C. Merz, H. Rodermond, et al. 2010. Wnt activity defines colon cancer stem cells and is regulated by the microenvironment. *Nat. Cell Biol.* 12:468–476. http://dx.doi.org/10.1038/ncb2048

Visvader, J.E., and G.J. Lindeman. 2008. Cancer stem cells in solid tumours: accumulating evidence and unresolved questions. *Nat. Rev. Cancer.* 8:755–768. http://dx.doi.org/10.1038/nrc2499

Voloshin, T., D. Alishekevitz, L. Kaneti, V. Miller, E. Isakov, I. Kaplanov, E. Voronov, E. Fremder, M. Benhar, M. Machluf, et al. 2015. Blocking IL1β pathway following paclitaxel chemotherapy slightly inhibits primary tumor growth but promotes spontaneous metastasis. *Mol. Cancer Ther.* 14:1385–1394. http://dx.doi.org/10.1158/1535-7163.MCT-14-0969

Wang, W.Y., C.C. Hsu, T.Y. Wang, C.R. Li, Y.C. Hou, J.M. Chu, C.T. Lee, M.S. Liu, J.J. Su, K.Y. Jian, et al. 2013. A gene expression signature of epithelial tubulogenesis and a role for ASPM in pancreatic tumor progression. *Gastroenterology.* 145:1110–1120. http://dx.doi.org/10.1053/j.gastro.2013.07.040

Yamauchi, K., M. Yang, K. Hayashi, P. Jiang, N. Yamamoto, H. Tsuchiya, K. Tomita, A.R. Moossa, M. Bouvet, and R.M. Hoffman. 2008. Induction of cancer metastasis by cyclophosphamide pretreatment of host mice: an opposite effect of chemotherapy. *Cancer Res.* 68:516–520. http://dx.doi.org/10.1158/0008-5472.CAN-07-3063

Zhang, M., A. Tsimelzon, C.H. Chang, C. Fan, A. Wolff, C.M. Perou, S.G. Hilsenbeck, and J.M. Rosen. 2015. Intratumoral heterogeneity in a Trp53-null mouse model of human breast cancer. *Cancer Discov.* 5:520–533. http://dx.doi.org/10.1158/2159-8290.CD-14-1101